DESIGNING AND CALIBRATING AN AEROSOL MEASUREMENT INFRASTRUCTURE IN LUTJEWAD

Stijn van Rijn
EES-2020

Master Programme Energy and
Environmental Sciences, University of Groningen

university of groningen / faculty of science and engineering / energy and sustainability research institute groningen

Research report of Stijn van Rijn

Report: EES-2020

Supervised by:
U. (Ulrike) Dusek, PhD, Center for Isotope Research (CIO)
dr. ir. H.A. (Bert) Scheeren, Center for Isotope Research (CIO)

University of Groningen
Energy and Sustainability Research Institute Groningen, ESRIG
Nijenborgh 6
9747 AG Groningen
T: 050 - 363 4760
W: www.rug.nl/research/esrig

University of Groningen

Faculty of Science and Engineering

Centre for isotope research

Designing and calibrating an aerosol measurement infrastructure in Lutjewad

Masterthesis

S.S.A. van Rijn - s2364026

January 28, 2020

Supervised by:

Ulrike Dusek, PhD

Assistant Professor of Centre for Isotope Research (CIO)

and

dr. ir. Bert Scheeren

Researcher and lab coordinator of Centre for Isotope Research (CIO)

1 Abstract

In this thesis an aerosol measurement infrastructure is designed for the Lutjewad station of atmospheric research. This infrastructure must constantly sample air from 20 meters height and transport the sample to the ground level. After an subsampling, the sample is transported through a sample pipe and a manifold to three measurement devices: a Scanning Mobility Particle Sizer, a Cloud Condensation Nuclei Counter and an Aerosol Chemical Speciation Monitor. Using theoretical equations of aerosol transport efficiency, a model is built to calculate the transport efficiency in the inlet as a result of particle loss due to diffusion, gravitational settling, impaction and isokinetic sampling. The particle transport efficiency from the sample pipe is also tested experimentally, focussing on losses due to diffusion. The actual aerosol transport efficiency was slightly lower compared to the theoretical values from the model. Since the model describes a perfect system, it represents the maximum theoretical efficiency. The lower aerosol transport efficiency was expected, for the inlet in reality in not perfect. A proper calibration with the entire infrastructure is advised for the future.

Contents

2 Introduction

2.1 Aerosol

The term of aerosol finds its origin in the Greek word "hydrosols", which means "water particle". This term is used to refer to a suspension of particles in water, or some other liquid. When particles are suspended in a gaseous medium, rather than in a liquid, one refers to aerosol. The particles in the aerosol can be either solid or liquid themselves (Kulkarni et al., 2011). The particles that are suspended usually have a wide range of particle sizes, a so called particle size distribution. Aerosol particles are typically in the range 1 nanometer to 100 micrometers, which are several orders of magnitude. The particles can come from all sorts of sources, both anthropogenic and natural sources. Some examples of anthropogenic aerosol sources are smoke from power generation, combustion engines and wood combustion. Some natural sources are for example the uptake of sea salt or dust, floating virusses and organic materials from trees. As a result of the various aerosol sources, the chemical composition of the particles varies as well. In figure 1 the diameters are displayed for some typical aerosol particles.

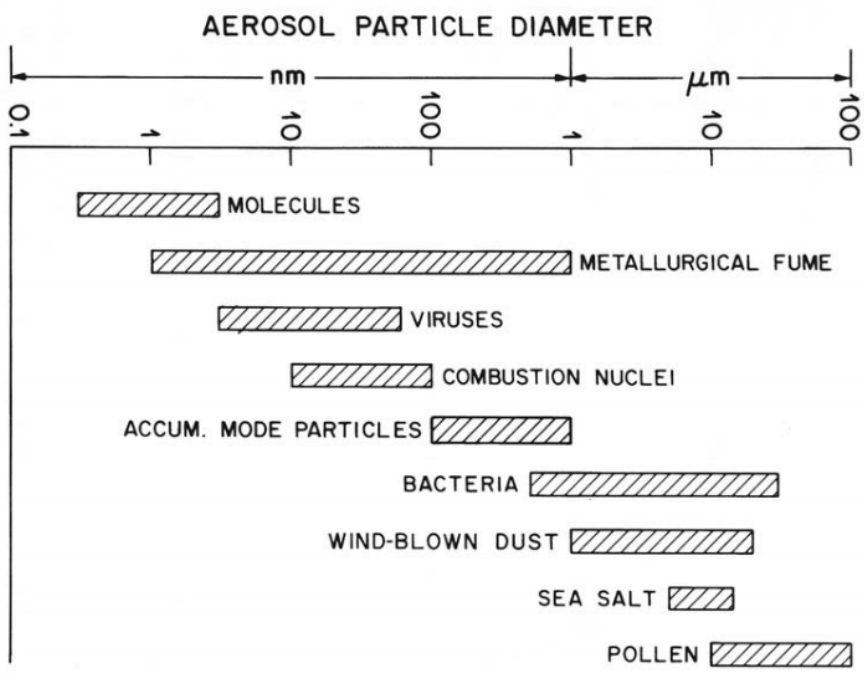

Figure 1: Particle diameters for several aerosol. From (Tiwary and Colls, 2010), page 58.

Another very famous example for aerosols are clouds. Cloud droplets are formed by condensation of water on existing solid or liquid aerosol particles, increasing the particle diameter.

2.2 Radiative forcing

The scientific concept behind climate change is called radiative forcing. This is the net result of the energy absorption and the energy radiated back to space in Watts per square meters. If there is a net positive radiative forcing, the climate temperature will increase and vice versa. Various parts of the environment affect the radiative forcing. The quantification of this radiative forcing due to various factors is shown in figure 2, (Brèon et al., 2013).

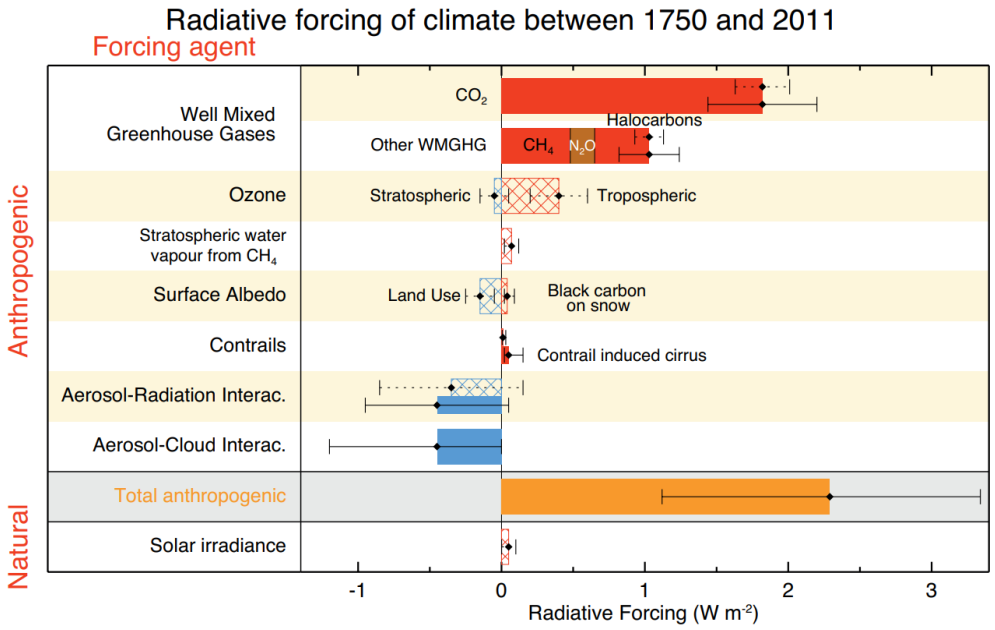

Figure 2: Net radiative forcing according to the fifth assessment of the Intergovernmental Panel on Climate Change (Brèon et al., 2013).

From figure 2 it is seen that aerosol has a direct and indirect influence on radiative forcing. Aerosol and clouds both have a negative net radiative forcing, while clouds are formed initially by aerosol itself (Tiwary and Colls, 2010)(Kulkarni et al., 2011). Clouds increase the albedo of the earth, inducing an higher reflectation of solar radiation. The uncertainty in the quantificationin for both aerosol effects however is substantial, making further research necessary. An example of such atmospheric research is done by the Ruisdael observatory.

2.3 Ruisdael observatory

The Ruisdael observatory is a Dutch collaboration of various institutes to research the atmosphere. The Ruisdael observatory is named after the Dutch painter Jacob van Ruisdael. He lived between 1629 - 1682 and was famous for his paintings of clouds (NWO, 2019). One of his paintings is seen in figure 3.

Figure 3: Windmolen van Wijk bij Duurstede by Jacob van Ruisdael. The clouds are very realistic. (franshalsmuseum.nl, 2019)

The university of Groningen is one of the partners in the Ruisdael observatory, together with the TU Delft, VU Amsterdam, Wageningen University, Utrecht University, TNO, KNMI and the RIVM. The Ruisdael observatory has 4 atmospheric research stations and it facilitates mobile research. The station in the north of Groningen is called Lutjewad. Lutjewad is located as close to the sea as possible, just behind the dike. The Lutjewad station still lacked a continuous aerosol measuremnt infrastructure, although aerosol measurement are an important factor of the Ruisdael observatory.

2.4 Objective for this project

In this project, an aerosol measurement infrastructure consisting of an inlet and a laboratorium is designed, constructed and tested for the Lutjewad station. The Ruisdael boundary conditions state that the aerosol sampling entrance has to be 10 meters above the ground. Since the dike is so close to the Lutjewad station, the top of the dike is considered as the ground level. This means that the aerosol sampling entrance should be 20 meters above the ground, for the dike is about 9 meter high. The focus in this project is mainly on the aerosol transport from the inlet to the measurement devices. The infrastructure is designed to maintain as much particles in the aerosol as possible. If the transport changes the aerosol greatly, the measurements would be false. However, since a perfect transport is impossible, the inlet is calibrated by measuring the particle losses for various particle sizes.

3 Theory

In this section some relevant aerosol dynamics will be explained. In general, the books Aerosol Measurement (Kulkarni et al., 2011) and Air Pollution (Tiwary and Colls, 2010) are used for this section. SI units will be used in the equations, e.g., m for length, kg for weight et cetera. If an equation uses different units, this will be mentioned specifically.

Particles in an aerosol have all sorts of interactions amongst themselves and their surroundings. This results in several changes in the particle size distribution and particle number concentration. When a particle collides with another particle or a wall, the particle will stick to it resulting in a decreased particle number concentration (particle loss). There are various particle loss mechanisms. The significance of these mechanisms varies with particle size, e.g., larger particles are lost by mechanism A, while smaller particles are lost by mechanism B. In this way, the composition of the aerosol is constantly changing.

3.1 Particle equivalent diameter

In order to compare the particles, a functional unit is chosen. Particle size is a very usefull unit, although it does not explain all the particle behavior. For example, two particles with different chemical composition or physical properties like density can display different behavior, despite their particle diameter is the same. To adress this problem, an equivalent particle diameter is used. This refers to the potential diameter of a particle that exhibits a specific type of behavior. For example, the aerodynamic equivalent diameter is the diameter of a spherical particle with a density of 1000 kg per cubic meter. This aerodynamic diameter is mainly used in this thesis.

3.2 Turbulent and laminar flow

In fluid dynamics, turbulent flow is defined as the chaotic flow, while laminar flow is the smooth flow. Particles in a turbulent flow will collide much more, resulting in a higher particle loss. The type of flow is calculated using the Reynolds number, as seen in equation 1 (Kulkarni et al., 2011).

$$Re = \frac{\rho_{air} v d}{\eta_{air}} \tag{1}$$

With Re as the dimensionless Reynolds number, ρ_{air} as the density of the gas, v as the velocity of the gas and d as the inner diameter of a circular tube and η_{air} as the viscosity of the air. The value of the dimensionless Re will indicate either a laminar flow ($R < 2000$) or a turbulent flow ($R > 2000$). Laminar flow will be assumed in the following particle loss principles, for the infrastructure is designed to house laminar flow. In this way the particle loss can be estimated in more detail.

3.3 Aerosol transport efficiency

When an aerosol is transported through a tube, a fraction of the particles will not reach the end of the tube due to particle loss mechanisms. The aerosol transport efficiency is the inverse of that particle loss fraction, as seen in equation 2.

$$\eta = 1 - p \tag{2}$$

Where η represents the transport efficiency as a percentage and p the fraction of particles that will not reach the end of the tube (i.e. particle loss) as a percentage. In the next subsections, some particle loss processes will be discussed and explained in more detail. For every particle loss process, an aerosol transport efficiency is found. (Kulkarni et al., 2011).

3.4 Diffusion

Particles suspended in a gaseous medium display a random movement, called the Brownian motion. If there is a concentration gradient, there will be a net flus of particles towards the low concentration. In a simple one-dimenstional case, the flux J in direction x is given by equation 3:

$$J = -D\frac{\partial C_p}{\partial x} \tag{3}$$

Where D is the diffusion coefficient, C_p the concentration of the particles. The diffusion coefficient for particles can be expressed as equation 4.

$$D = \frac{kTC_c}{3\pi\eta_{air}D_p} \tag{4}$$

With k the Boltzmann constant ($1.38 \times 10^{-23} NmK^{-1}$), T the temperature of the air, η_{air} the viscosity of the air, D_p the particle diameter, C_c a slip correction factor. To further understand and use these equations, the slip correction factor C_c should be explained. It is however convenient to first define the Knudsen number Kn, as seen in equation 5.

$$Kn = \frac{2\lambda}{D_p} \tag{5}$$

D_p is the particle diameter again, while λ represents the mean free path of the gas molecules. This is the average distance a gas molecule travels between collisions with other gas molecules. The Knudsen number is used as an indicator. A high Kn ($Kn \gg 1$) means that aerosol particles are small compared to the mean free path of the air. A low Kn ($Kn \ll 1$) means that the particles are so large that they experience many molecular collisions in a short time and hence experience the surrounding gas as a contiuum flow.

Moving back to the slip factor C_c. Small particles tend to experience individual molecular collisions, which reduces the drag force of the fluid on the particles compared to the contiuum case ($Kn \gg 1$). For a given external force, smaller particles move therefore

faster compared to larger particles. A correction factor is determined to correct for this phenomenon by (Allen and Raabe, 1985), as seen in equation 6

$$C_c = 1 + Kn[\alpha + \beta e^{\frac{-\gamma}{Kn}}] \tag{6}$$

With Kn as the Knudsen number and α, β and γ as empirical parameters depending on the type of particles and the medium. For now, a mean free path of $\lambda = 0.0664\ \mu m$ is used, since this is oftenly used in the standard (NTP) situation. For solid particles, the parameters are $\alpha = 1.142$, $\beta = 0.558$ and $\gamma = 0.999$ (Allen and Raabe, 1985). With these assumptions, equation 6 can be rewritten in equation 7:

$$C_c = 1 + \frac{1}{PD_p}[15.60 + 7.00e^{-0.059PD_p}] \tag{7}$$

With P as the absolute pressure in kPa and D_p as the particle diameter in μm. Obviously, equation 7 implies that C_c is large for small particles and vice versa.

In order to quantify the particle loss by diffusion, the laminar flow case is used (Gormley and Kennedy, 1948). The particle loss is estimated by calculating an efficiency of a pipe with length L and mass flow Q. This case is displayed in equation 8.

$$\eta_{diff} = \begin{cases} 1 - 2.56\ \xi^{\frac{2}{3}} + 1.2\ \xi + 0.177\ \xi^{\frac{4}{3}} & \text{for } \xi < 0.02 \\ 0.819\ e^{-3.657\xi} + 0.097\ e^{-22.3\xi} + 0.032\ e^{-57\xi} & \text{for } \xi > 0.02 \end{cases} \tag{8}$$

With η_{diff} as the transport efficiency due to diffusion and ξ as a dimensionless variable defined in equation 9.

$$\xi = \frac{\pi DL}{Q} \tag{9}$$

D represents the diffusion coefficient, L the length of the pipe and Q the mass flow inside the pipe. Using equation 8, the expected particle loss by diffusion can be estimated in all tubes with a circular cross section housing laminar flow. The aerosol particles close to the wall are diffused towards the wall and deposited.

3.5 Gravitational settling

The particles of an aerosol are affected by the gravitational force of the earth. Especially the heavier particles can be deposited by gravity. Particles will not reach the measurement devices when deposited in the tubing leading to the instrument, leading to particle loss. Logcially, gravitational settling will only occur in horizontal tubes.

The vertical velocity induced by gravity is called terminal settling velocity, v_t, and is given in equation 10 (Tiwary and Colls, 2010):

$$v_t = \tau\ g \tag{10}$$

With g as the gravitational constant being 9.81 $m\ s^{-2}$ and τ as the relaxation time. Relaxation time refers to the amount of time in which particles achieve a constant velocity

relative to the carrier gas after being affected by an external force. The relaxation time is given by equation 11 (Tiwary and Colls, 2010).

$$\tau = \frac{\rho_p D_p^2 C_c}{18\eta_{air}} \tag{11}$$

In this equation, ρ_p represents the density of the particle, D_p the particle diameter, C_c the slip correction factor (equation 7) and η_{air} the viscosity of air, being $1.825 \cdot 10^{-5} kg\ m^{-1} s^{-1}$ for standard parameters. The physical dimensions of the tube itself are therefore important as well.

The efficiency with respect to gravitational losses of aerosol transport through a horizontal tube with a circular crosssection is given by equation 12 (Kulkarni et al., 2011).

$$\eta_{grav} = e^{\frac{-dLv_t}{Q}} \tag{12}$$

With η_{grav} as the efficiency by gravitational settling, d as the inner diameter of the aerosol tube, L the length of the aerosol tube, Q the mass flow and v_t the terminal settling velocity.

3.6 Impaction

When an aerosol transporting tube makes a turn, the particles have to follow the airflow around the turn. Particles cannot however follow the gaseous medium as easy as the gas molecules itself, for the moment of inertia is larger for a heavier particle. In figure 4 a schematic figure of such a turn is seen.

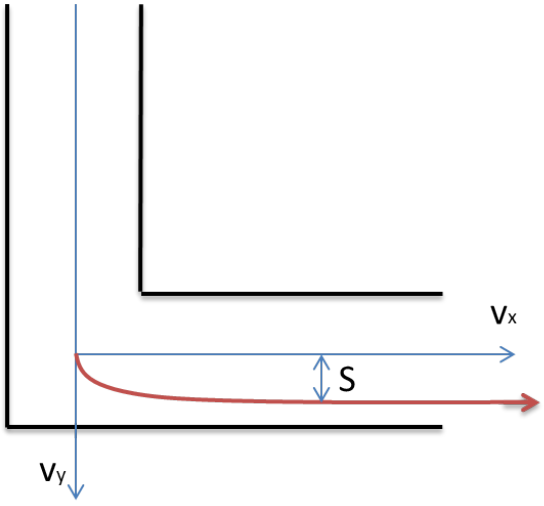

Figure 4: Schematic representation of a turn in a tube transporting aerosol. The velocity of the flow is changes from the y-direction (v_y) to the x-direction (v_x). Due to the moment of inertia, particles can be displaced in the tube. This is displayed by the stopping distance S.

Figure 4 shows a turn of velocity from the y-direction (v_y) to the x-direction (v_x). Particles with a larger inertia tend to have a wider bend around the corner, displacing

them inside the tube. This displacement distance is called the stopping distance S. The stopping distance can be calculated by equation 13 (Tiwary and Colls, 2010).

$$S = v_0 \tau \tag{13}$$

With v_0 as the initial velocity in the initial direction and τ as the relaxation time from equation 11. Since τ depends on the particle density and diameter, the stopping distance depends on particle density and diameter as well. Heavier, larger particles have a larger stopping distance compared to smaller, lighter particles.

If the stopping distance is larger than the initial distance of the particle from the tube wall, the particles are impacted on the wall of the tube, causing particle loss. If the assumption is made that the aerosol is distributed evenly across the tube, the fraction of the aerosol particles that flow within their stopping distance along the outer wall of the tube, gets impacted after the turn. This is visualized in figure 5 for particles with the same aerodynamic diameter.

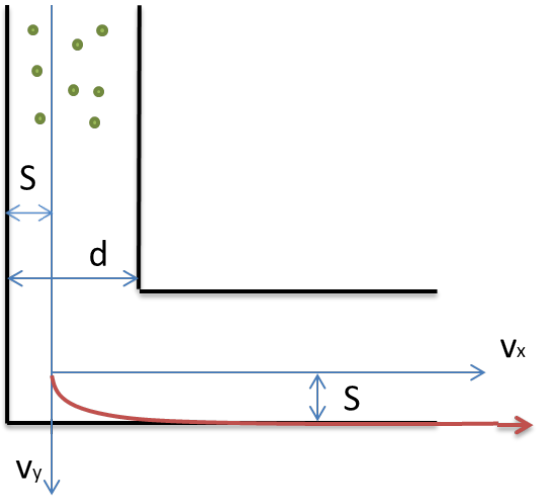

Figure 5: An example of impaction. The green dots represent particles in the flow, with S as the stopping distance and d as the diameter of the tube. In this case, 3 of the 8 particles will be impacted.

Figure 5 shows the fraction of the particles that will be impacted after the turn. As seen from figure 5, the efficiency of the aerosol transport depends on the stopping distance and the inner diameter of the tube d. The impaction however is calculated for the diameter of a tube with a square crossection, hence the inner diameter is to be corrected for the circular tube. This correction factor is the relative difference between the areas of a square and a circle, being $\frac{\sqrt{\pi}}{2}$. The efficiency by impaction in a circular tube is seen in equation 14.

$$\eta_{imp} = \frac{\sqrt{\pi} d - 2S}{\sqrt{\pi} d} \tag{14}$$

In this equation represents η_{imp} the efficiency of the aerosol transport with respect to impaction in a circular tube with a 90 ° turn. d stands for the circular inner diameter of

the tube and S stands for the stopping distance can be seen in equation 13.

3.7 Isokinetic subsampling

Sometimes it is convenient to subsample from the existing sample by placing a smaller tube in the larger tube. In this way, the main sample is divided in the subsample and some rest sample.

While making a subsample, particle loss can occur. When the initial flow velocity is equal to the subsample flow velocity, the subsampling is called isokinetic. The streamlines of the flow will not be altered. If the initial velocity differs from sample velocity, the streamlines of the flow will be altered. The particles in the flow must follow the streamlines, although the particles will need some time to adapt, similar to the stopping distance as in equation 13. In figure 6 a schematic representation is given for this phenomena.

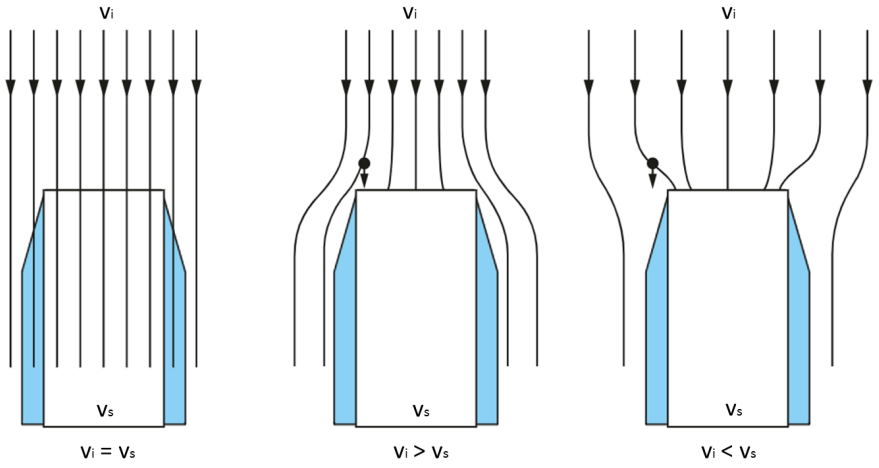

Figure 6: From left to right: Isokinetic sampling, Sub-isokinetic sampling and Super-isokinetic sampling. v_i and v_s are respectively the inital and subsample velocity. Adjusted from (Sigrist, 2019).

Subsampling for three isokinetic conditions is shown in figure 6. Logically, particles with a larger moment of inertia will find more difficulty to follow the altering streamlines, disturbing the size distribution of the subsample. The efficiency for this particle loss is given in equation 15 (S.P. Belyaev, 1974).

$$\eta_{iso} = \begin{cases} 1 + \frac{\frac{v_i}{v_s} - 1}{1 + \frac{0.418}{Stk}} & \text{for } \frac{v_i}{v_s} > 1 \\ 1 & \text{for } \frac{v_i}{v_s} = 1 \\ 1 + \frac{\frac{v_i}{v_s} - 1}{1 + \frac{0.506\sqrt{v_i/v_s}}{Stk}} & \text{for } \frac{v_i}{v_s} < 1 \end{cases} \tag{15}$$

In this equation, v_i represents the initial velocity before subsampling, v_s represents the velocity of the subsample and Stk is a dimensionless number called Stokes number. Stokes number can be calculated by equation 16 (Kulkarni et al., 2011).

$$Stk = \frac{\tau v_i}{d} \tag{16}$$

Where τ is the relaxation time as in equation 11, v_i is the inital flow velocity before subsampling and d the diameter of the subsampling tube.

The efficiency due to isokinetic sampling from equation 15 only holds for $0.01 \leq Stk \leq 100$ and $0.1 \leq v_i/v_s \leq 10$.

3.8 Total efficiency

The total efficiency is simply the product of all the efficiencies from the phenomena explained above. The equation for the total efficiency is seen in equation 17.

$$\eta_{tot} = \eta_{diff}\eta_{grav}\eta_{imp}\eta_{iso} \tag{17}$$

With η_{diff} the efficiency due to diffusion as in equation 8, η_{grav} the efficiency due to gravitational settling as in equation 12, η_{imp} the efficiency due to impaction as in equation 14 and η_{iso} the efficiency due to isokinetic subsampling as in equations 15.

3.9 Statistical analysis

To test the particle loss model, an experimental test will be performed to learn the aerosol transport efficiency of the inlet (chapter 6). In order to discuss the data, a statistical analysis is necessary. The theory and equations for this section are used from the book (Ott and Longnecker, 2001).

Due to the variable concentration of aerosol, many measurements are needed to find the particle loss. The measurements are done by taking samples from the outside air. In statistical terms, the outside air is the population, from which samples are taken. Ideally, one could analyze the whole population, but this is not realistic for air measurements.

When several measurements are taken on one sample, a mean value can be calculated. Many samples are taken, in order to minimize the error. These samples have their own means. All the possible means for a certain sample size can be represented in a sampling distribution. This sampling distribution is a probability density of finding a specific sample in the population. The standard deviation of this sampling probability density is called the standard error. This standard error can be calculated by equation 18.

$$\sigma_{\bar{x}} = \frac{\sigma}{\sqrt{N}} \tag{18}$$

With $\sigma_{\bar{x}}$ as the standard error, σ as the true standard deviation of the population and N as the number of data points in the sample. It is seen that the standard error decreases as the number of data points increases. There is one problem with the σ however, since the true standard deviation of the population is only known if the whole population is sampled. One could approximate the standard error by using the sample standard deviation instead of the true population standard deviation. This is seen in equation 19.

$$\sigma_{\bar{x}} \approx \frac{s}{\sqrt{N}} \tag{19}$$

The standard error can only be used if the measurements are independent. This means that there is no drift or trend in the population over time. Uncertainties such as the standard deviation or the standard error are crucial to give the right amount of credibility to the measurements. The propagation of these uncertainties must be considered when the data is used. This is called error propagation or propagation of uncertainty. The error propagation is calculated using equation 20:

$$s_f = \sqrt{\left(\frac{\partial f}{\partial x}\right)^2 s_x^2 + \left(\frac{\partial f}{\partial y}\right)^2 s_y^2 + \left(\frac{\partial f}{\partial z}\right)^2 s_z^2 + ...} \tag{20}$$

Where s_f is the uncertainty in the function $f(x, y, z, ...)$ and s_x, s_y, s_z, ... are the uncertainties in respectively x, y, z and so on.

4 The aerosol infrastructure in Lutjewad

In this chapter, the aerosol infrastructure in Lutjewad is discussed. Starting from the requirements, the aerosol infrastructure is designed and eventually constructed. Only the final aerosol infrastructure will be explained, passing over many intermediate plans between the initial and final infrastructure. Pictures of the parts and the construction of the aerosol infrastructure can be found in table 2 in the Appendix, chapter 11, as well as a list of companies that provided parts or services for the aerosol infrastructure. The construction is not yet completed.

4.1 Requirements

In order to make proper aerosol measurements, the sample entrance height should be 10 meters above the ground. Since there is a dike close to the Lutjewad station, the sample entrance must be 10 meters above the height of the dike. The dike is 9 meters high, thus the sample entrance should be around 20 meters high. At the Lutjewad station, there is already a tower for other atmospheric measurements. It is therefore convenient to attach the new aerosol pipe to the existing tower, for the measurement devices cannot be placed in the tower themselves. Neither can the aerosol be transported to the Lutjewad main building, as this building is placed too far fromthe tower. To house the measurement devices, a new laboratorium will be placed just next to the tower.

Since the tower is next to the sea, the whole aerosol infrastructure should be stormproof and filter out most of the salt particles. Salt particles can damage the measurement devices and dryers, which intensifies the maintenance necessities.

Maintenance itself is an important factor as well. The ideal aerosol infrastructure would imply that maintenance is easy and not a lot of work. This means that parts should have a high quality, are easily ordered and can be removed and replaced part by part. Technicians should be able to disassemble the aerosol infrastructure in order to perform maintenance or replace certain parts.

The amount of sample flow is important as well. Measurement devices need a certain amount of flow to analyze the aerosol. The total sample flow should be enough to feed all the measurement devices, yet should also preserve availability for additional measurement opportunities in the future. For the aerosol measurement infrastructure is not only designed for the current requirements, it should have space for future additions.

4.2 General overview of the infrastructure

A general overview of the new aerosol infrastructure is shown in figure 7 and discussed below.

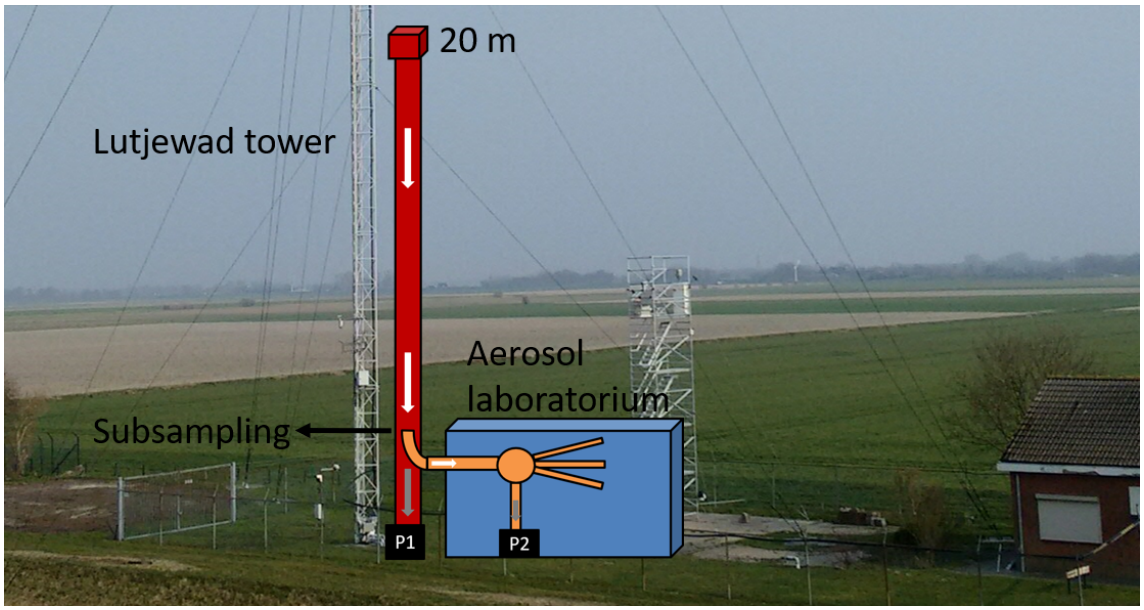

Figure 7: Schematic overview of the new aerosol measurement structure, drawn on a picture of the Lutjewad station. The (red) aerosol main pipe can be attached to the existing Lutjewad tower. A new laboratorium must be placed near the main pipe to minimize horizontal transport. Using a (orange) sample pipe, a subsample is transported to measurement devices. P1 and P2 represent the pumps that create the flow through the system.

As displayed in figure 7, a whole new infrastructure is designed next to the existing Lutjewad tower. The whole aerosol infrastructure can be considered as the combination of the laboratorium and the inlet. The aerosol inlet is defined as the parts from the sample entrance untill the measurement devices. A subsampling sample pipe is shown in orange, transporting the sample through the laboratorium wall to the measurement devices. This subsampling is done at the centre of the main pipe, for most of the particle loss occurs at the walls. Subsampling is also convenient to manage the suitable amount of sample into the laboratorium.

4.3 Design of the aerosol inlet

In this section, the design of the aerosol infrastructure will be described and displayed in schematic figures. The focus will be on the connections and the overall use of the aerosol infrastructure. The entire aerosol infrastructure is divided in two subparts: The outer part of the aerosol inlet (section 4.3.1) and the inner part of the aerosol inlet (section 4.3.2). More information about the individual parts in the aerosol infrastructure are explained in section 4.4.

4.3.1 Outer part of the inlet

The outer part of the inlet is defined as the part that is outside the aerosol laboratorium. A schematic figure is displayed in figure 8.

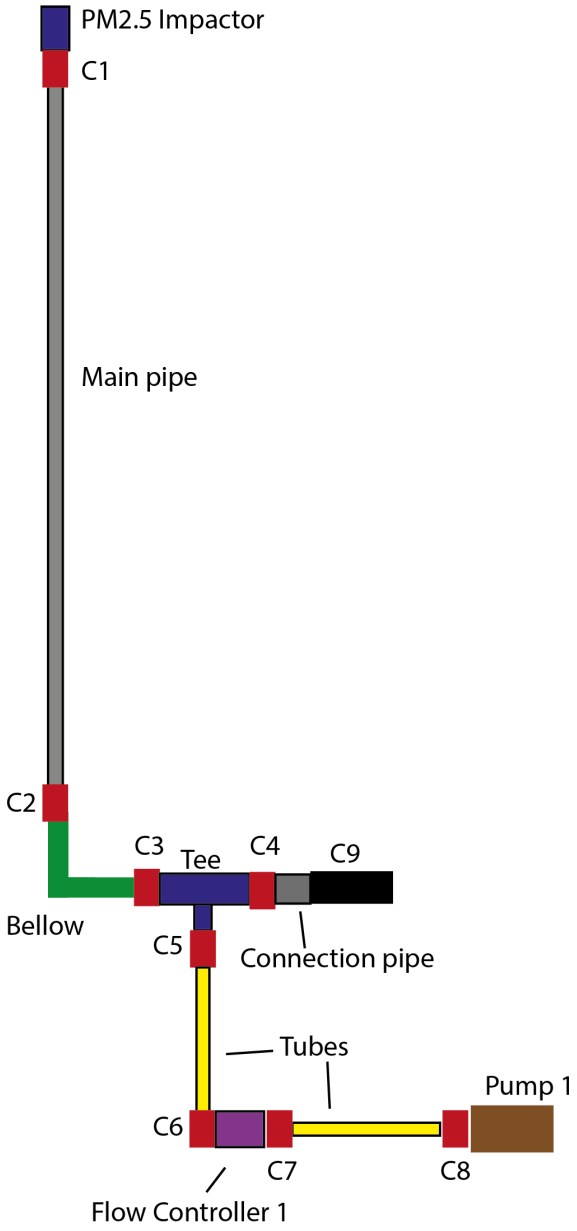

Figure 8: Schematic representation of the outer part of the inlet. This part starts from the sample impactor and includes the main pipe. Connectors are shown in red and marked with a letter C. The figure is not to scale.

Figure 8 will be discussed from top to bottom. On top of the inlet at a height of 20 meters, there is a PM2.5 aerosol impactor to eliminate particles larger than 2.5 μm. Ambient air is drawn through the impactor which has an outlet diameter of 32 mm. Since the main pipe has an outer diameter of 50 mm, connector C1 is used to connect the impactor pipe and the main pipe. This means that C1 is a reducing union from 50 mm

to 32 mm, custom made by the company Swagelok. A small connection pipe (not shown in the figure) is placed between the inlet and connector C1. The main pipe is 18 meters long and is attached to the existing Lutjewad tower. At the bottom of the main pipe, a DN50 flange is welded. The bellow is a 500 mm long, flexible part with DN50 flanges at either end. The bellow is used to compensate for vibrations by the weather, while making a 90° turn. This turn is needed to transport the aerosol to the measurment devices in the laboratorium. The bellow is connected with C2 and C3 to respectively the main pipe and the t-connector. Since the all these parts have DN50 flanges (made by the company Pfeiffer Vacuum), C2 and C3 are just clamps with o-rings. Connector C4 is a similar clamp. This connection pipe consists of a DN50 flange, welded to a pipe with an outer diameter of 1.5 inch. Connection C9 closes off the outer part and beginning the inner part of the inlet. This is displayed more clearly in figure 9. C9 is a reducing union, also from Swagelok, from 1.5 inch to 1 inch.

The bottom part of the t-connector is used to connect the inlet to the pump. It is connected to a $\frac{1}{2}$ inch tube. Connector C5 is therefore a combination of connectors going from DN50 to a $\frac{1}{2}$ inch end. The first tube is attached to the first flow controller, using connector C6. The flow controller has a $\frac{1}{4}$ inch inlet, so C6 is a $\frac{1}{2}$ inch to $\frac{1}{4}$ inch connection. The second tube is a $\frac{1}{4}$ inch tube connecting the flow controller to the first pump. Connectors C7 and C8 are both $\frac{1}{4}$ inch connections to complete the outer part of the inlet.

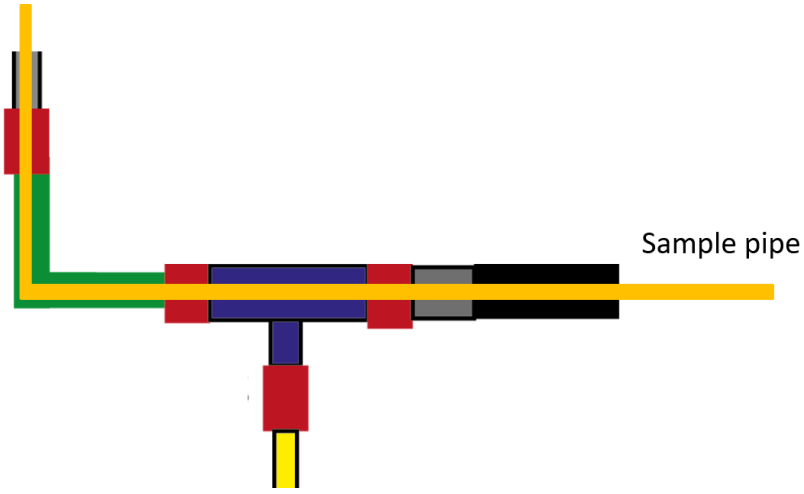

Figure 9: The placement of the sample pipe in the outer part of the inlet. This figure is a zoom of figure 8 with the addition of the sample pipe, explained in the inner part of the inlet (4.3.2).

Figure 9 displays the placement of the subsampling system. The sample pipe is placed partly inside the outer inlet, going through connectors C2, C3, C4 and C9, the t-connector (tee), the bellow and the connection pipe.

4.3.2 Inner part of the inlet

The inner part of the inlet is defined starting from the subsampling to the measurement devices. A large part of the inlet is placed in the laboratorium as well. In figure 10 the schematic represenatation is seen. This is not to scale.

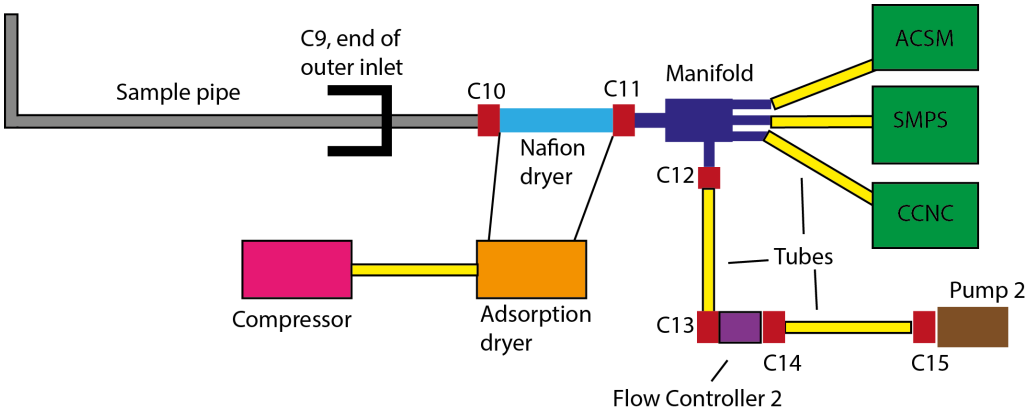

Figure 10: Schematic representation of the inner inlet. This part starts from the sample pipe and includes the manifold. The C-series are all sorts of connectors. The figure is not on scale.

Figure 10 will be discussed from left to right. The largest part of the inner inlet is the sample pipe. This is a pipe with a 1 inch outer diameter and is 2 meters long. After the first 50 mm, the pipe is bent into 90 ° turn. The sample pipe is placed inside the outer inlet, going through connector C9 (indicated by the black part), the tee and the bellow from figure 8. The bellow follows the bend of the sample pipe. The vertical part of the sample pipe fits inside the main pipe and reaches higher than connector C2, as shown in figure 9. The sample pipe subsamples the air from the main pipe and transports the sample towards the laboratorium (not displayed in figure 10). Inside the laboratorium, the sample pipe is attached to a nafion dryer, using connector C10. Since a nafion dryer needs dry air to succesfully dry the aerosol, an adsorption dryer is connected with the nafion dryer. The working principle of a nafion dryer is explained further in section 4.4.3. The adsorption dryer receives compressed air from a compressor.

The sample is now dried and transported, via connector C11, to the manifold. The manifold is used to split an aerosol sample isokinetically to several outlets. This is used to simultaneously provide several measurement devices from the same aerosol sample. There are three measurement devices (Scanning Mobility Particle Sizer, Cloud Condensation Nuclei Counter and Aerosol Chemical Speciation Monitor) displayed in figure 10, although the manifold has more outlets. In the future, more devices can be attached to this inlet. More information about the measurement devices is given in respectively sections 4.4.7, 4.4.8 and 4.4.9.

At the bottom part of the manifold, a bypass is seen. This bypass is used to pump away excess air. This excess air is the sample surplus that is not consumed by the measurement

devices. A $\frac{1}{4}$ inch tube connects the bypass with the flow controller using connectors C12 and C13. Since the bypass itself has an outer diameter of $\frac{3}{8}$ inch, connector C12 is a reducing union from $\frac{3}{8}$ inch to $\frac{1}{4}$ inch. The second flow controller has - like the flow controller in the outer part of the inlet - $\frac{1}{4}$ inch connections. Lastly, a $\frac{1}{4}$ inch tube connect the flow controller to the second pump, using connector C15. This is merely a $\frac{1}{4}$ inch to $\frac{1}{4}$ inch connector, similar to connector C8 from the outer inlet.

4.4 Part by part analysis

In this section, some parts mentioned in the outer and inner inlet (sections 4.3.1 and 4.3.2) will be further discussed. The three measurement devices will be explained roughly, without too much detail, since it was beyond the scope of this thesis.

4.4.1 PM2.5 impactor

The purpose of the PM2.5 impactor is to sample aerosol from the environment. In the essence, an aerosol impactor uses impaction (as explained in section 3.6). The working principle is seen in figure 11.

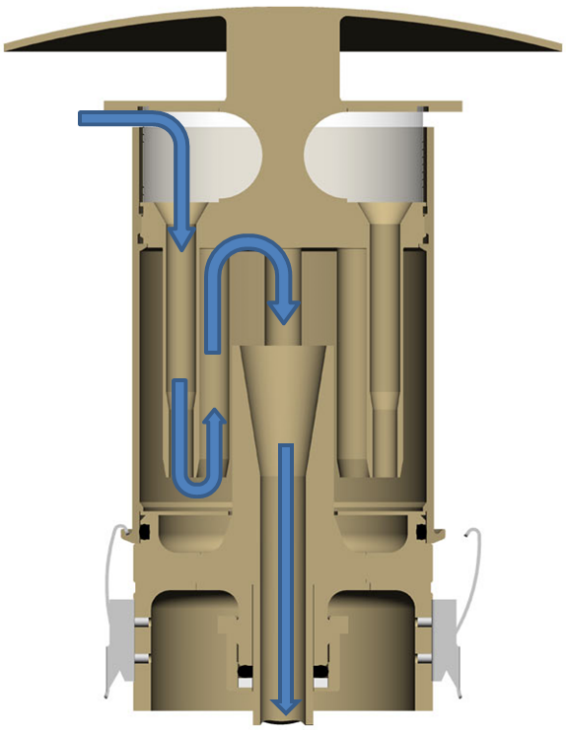

Figure 11: Schematic display of an aerosol impactor cross section. The blue arrows indicate the flow of air through the impactor. Image taken from (Digitel, 2019).

As shown in figure 11, air enters the impactor through a circular opening at the top and is channeled through several impaction jets, that accelerate the air flow towards a horizontal impaction plate. For clarity, only one jet is shown, although the impactor has many. At the exit of the jet, the air stream hits the impaction plate and makes a sharp

turn upward, resulting in possible impaction. Then, the air from all the jets is directed back downwards to the middle outlet. Equation 14 shows that larger particles will be deposited and the smaller particles will be able to follow the air stream. In this way, the impactor can be used to sample a particle below a certain cut-off size. The impactor works optimally for a fixed sample flow.

For this inlet, a PM2.5 impactor is used, i.e., particles larger than 2.5 $/mu$m are impacted. This means that most of the sea salt particles are excluded in the inlet. The impactor works optimally for a sample flow of 2.3 cubic meters per hour (38.33 liters per minute). This determines the flow in the main pipe. The aerosol impactor is bought from the company Digitel.

4.4.2 Main pipe

The main pipe is used to transport the sample flow towards the ground level. Ideally, a uniform pipe is used, for any impurity or edge can induce turbulance. When turbulance is introduced, particle loss will increase. Besides turbulance, particles can be deposited on edges as well, decreasing the transport efficiency. Another requirement for the main pipe is to be conductive. A non conductive material can become static, creating a potential to charged particles. This leads to more particle loss as well.

Regarding the material, stainless steel is used. Stainless steel does not corrode very quickly and it will not develop a static charge. Since it was not possible to buy a $\pm$ 20 meters long stainless steel pipe, 3 smaller pipes of 6 meters where used to weld the main pipe. To reduce welding edges, orbital welding is used. Orbital welding is a technique where the weld is applied without pause for the entire 360° of the pipe, while the pipe itself is filled with gas. Orbital welding is seen as one of the highest quality welding. The DN50 flange at the bottom the main pipe is welded conventionally since the subsampling is done before and the air is this part of the pipe is only transported to the pump. Besides, an orbital weld is harder and more expensive. Pictures of the weld and the main pipe are placed in the Appendix, chapter 11. The company PMF constructed and welded the main pipe.

4.4.3 Nafion dryer

The principle of a nafion dryer is schematically shown in figure 12.

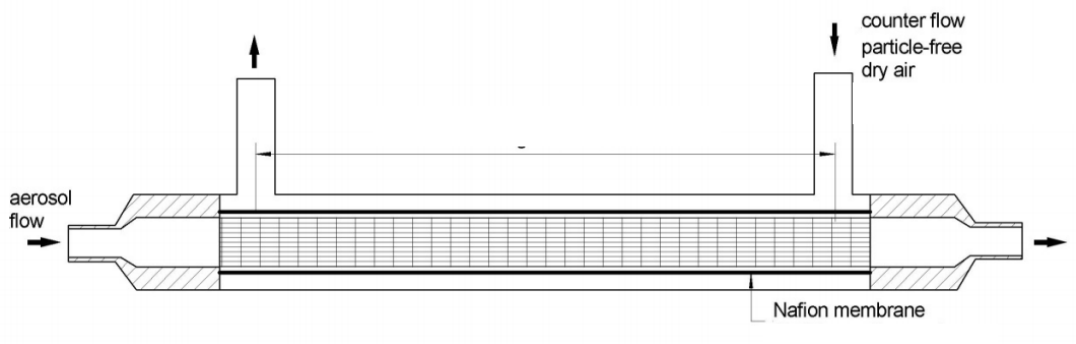

Figure 12: Schematic display of a nafion dryer cross section. The aerosol sample flow is dried by the dry counter flow. Image taken from (Wiedensohler and Birmili, 2019).

The aerosol sample is transported from left to right in figure 12. Inside the column a nafion membrane is placed. This membrane is transparant for water, while it is sealed for aerosol particles. At the top right corner, a counter flow is introduced at the opposite side of the membrane. The counter flow is dry, in contrast to the sample flow. Water vapor diffuses from the aerosol sample flow to the dry counter flow through the membrane due to the water vapor gradient. In this way, the sample flow is dried without losing particles. An oil-free compressor and an adsorption dryer are used to provide the dry air for the counter flow.

The degree of drying depends on several factors. If the counter flow is increased, the water vapor gradient will be larger, resulting in a higher degree of drying. A longer column exposes the aerosol sample longer to the water vapor gradient, also resulting in a dryer sample. The smaller the gradient, however, the less efficient is the drying. The nafion columns are made by the scientific institute Tropos. The adress can be found in the Appendix, chapter 11.

4.4.4 Manifold

The manifold is designed and manufactured by the company Tropos. To account for future additional instruments, the manifold has 7 exits: 6 of them have an outer diameter of $\frac{1}{4}$ inch and the last one is $\frac{1}{2}$ inch. To split the sample isokinetically, the manifold needs a flow rate of 16.7 liters per minute. A different flow rate results in a suboptimal isokinetic subsampling, i.e., either superisokinetic or subisokinetic subsampling (as explained in section 3.7). To assure the sample flow, the total sum of outflow will have to be 16.7 liters per minute. This means that the flow through the bypass is defined as 16.7 minus the the sample inlet of the measurement devices combined. A picture is placed in the Appendix.

4.4.5 Sample pipe

Since the manifold works optimally with a 16.7 liter per minute sample flow, the flow inside the sample pipe is fixed to be exactly the same. Regarding the material of the

sample pipe, the requirements are similar to the main pipe. Since the sample pipe is only 2 meters, a uniform stainless pipe is used. An outer diameter of 1 inch and a pipe thickness is 1mm is chosen to assure a laminar flow. The angle in the sample pipe is bent as smoothly as possible, avoiding impurities as much as possible. Realistically, the pipe will still be slightly deformated and ridged as a result of the bend. As explained in sections 4.4.1 and 4.4.4, the flows in the main pipe and sample pipe are fixed. Given the chosen diameters of the pipes, the velocities of the sample in both pipes are fixed. From the elaboration in section 3.7 about isokinetic subsampling, the only degree of freedom left to ensure isokinetic subsampling is the diameter of the sample pipe inlet. Assuming a 38.33 liters per minute flow in the main pipe with 46 mm inner diameter, combined with a 16.7 liters per minute flow through the 23.4 mm inner diameter of the sample pipe, the subsampling is superisokinetic (equation 15). To minimize particle loss, a conic part is welded on top of the sample pipe. This conic part has a inner diameter of 27 mm. Although the subsampling will still be superisokinetic with the conic addition, the particle loss is minimalized. The company Swagelok built the pipe with the bend.

4.4.6 Flow controllers and pumps

As explained in the sections above, the flow inside some parts needs to be maintained at a stable rate. The flow is induced by the pump and must be regulated and kept stable by a flow controller. For this inlet, downstream flow controllers are used. This means that the flow controllers control the flow at their outlet. The pumps, stationed after the flow controllers, will pump the air through the whole inlet. The capacity of the pumps is higher than the sample flow itself, creating an underpressure in the tube between the flow controllers and the pumps. Hence, it is chosen to use vacuum pumps for this inlet. The first pump, used in the outer inlet (figure 8) has a pump capacity of 4.1 cubic meters per hour (68.33 liters per minute). The accessory flow controller can be used up to 50 liters per minute. To account for possible future additions, higher capacities of both the flow controller and the vacuum pump are deliberately taken. In this way, it is possible to increase the total sample flow by changing the aerosol inlet or calculating the extra losses by impaction in the aerosol inlet.

The second flow controller and pump are overqualified as well. The pump can pump 1.9 cubic meters per hour (31.67 liters per minute), while the flow controller is capped at 20 liters per minute. Flow controllers need a certain pressure difference between upstream and downstream. For this smaller flow, this pressure difference is rather small. Therefore, a special Whisper version flow controller is used. The flow controllers are from the brand Alicat, bought from the company Inacom. The pumps from the company Becker DVP.

4.4.7 SMPS

SMPS is the abbreviation of Scanning Mobility Particle Sizer. A SMPS is used to scan a sample and measure the particle sizes of the aerosol in the sampled air. This particle size is measured based on the electrical mobility of the particles, making use of the electrical mobility equivalent diameter instead of the aerodynamic equivalent diameter. In principle, a SMPS is the combination of a consecutive Differential Mobility Analyzer (DMA) and a Condensation Particle Counter (CPC). A DMA selects monodisperse aerosol of a certain size, while the CPC counts the amount of particles in that size class. A schematic representation of the working principle of a DMA is diplayed in figure 13.

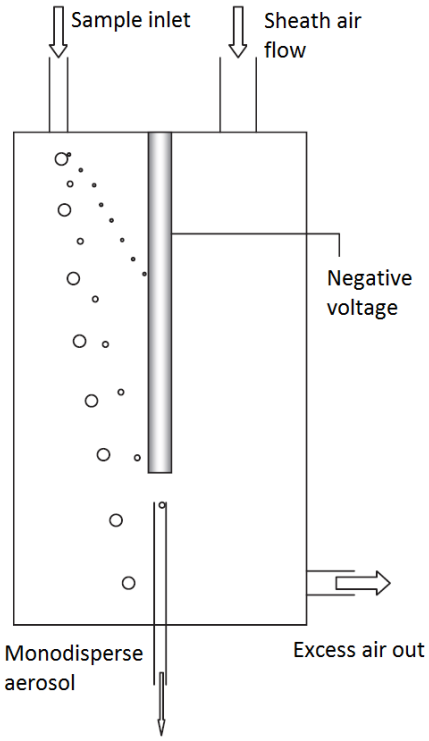

Figure 13: The working principle of a DMA. The (charged) sample and sheath flow are mixed in the column. For every voltage on the central rod, a certain particle size will reach the outlet through the slit. Image from (Tiwary and Colls, 2010)

Prior to the entrance of the DMA, the aerosol particles are charged by a radioactive source (e.g. ^{85}Kr). The charged particles are tranported into the column and mixed with a sheath air flow. This sheath air flow is a particle free flow of roughly ten times the sample flow. In the middle of the column, a rod is placed. This rod is charged with a negative voltage, inducing a potential between the rod and the charged particles. For every specific voltage, a certain particle diameter will enter the bottom outlet at the centre. The outgoing sample aerosol is now a monodisperse aerosol. The rest of the outflow is filtered and used as sheath flow again. The particle diameter can be calculated by equation 21 (from (Tiwary and Colls, 2010)).

$$Dp = \frac{EeC_c}{3\pi\eta_{air}v_{drift}} \tag{21}$$

With Dp as the particle diameter, E the electric field, e the electron charge, C_c the correction slip factor from equation 7, η_{air} the viscosity of the air and v_{drift} as the drift velocity of the particle. The electric field strength E scales with the voltage, which is applied to the centre rod. This voltage can be kept stable to focus on a specific particle diameter, or it can be scanned from a low voltage to a high voltage. The aerosol sample is then scanned for the whole size distribution.

The now monodisperse aerosol is transported to the CPC. This is a device that can count the amount of particles.

By combining a DMA and a CPC, the SMPS measures size distributions of the sampled aerosol: The DMA selects the particle size and consequently the CPC counts the amount of particles. Most SMPS's can measure particle diameters up to roughly 800 nm, starting from 10 nm or even smaller particle sizes. Hence, the SMPS is mainly used for smaller particles, below PM1. The SMPS is calculated to need a sample flow of 0.5 liters per minute.

4.4.8 CCN Counter

The CCN Counter (Cloud Condensation Nuclei Counter) is a device that counts the number of cloud droplets that are condensed on the sample aerosol for different levels of supersaturation. In other words, this device takes the aerosol sample and measures the amount of cloud particles formed on the sample aerosol for various supersaturation levels. The supersaturation is achieved by a column, which is schematically displayed in figure 14.

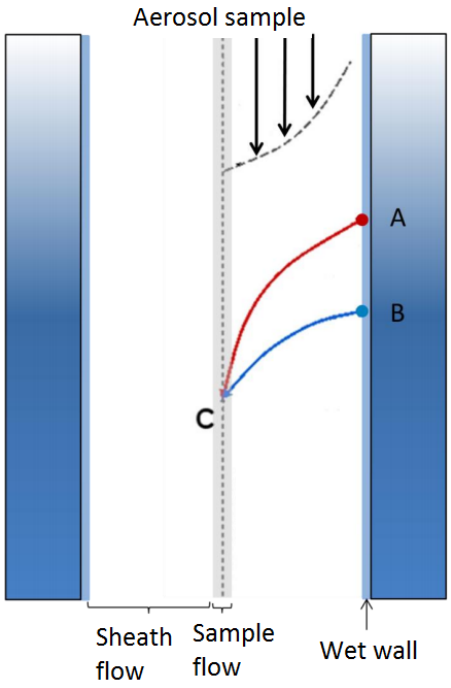

Figure 14: The working principle behind the creation of supersaturation in a CCN counter. The water vapor drifts from point B to point C quicker than the heat diffusion from point A to point C. Image from (DMT, 2012)

The aerosol sample is transported in the middle of the column, with a sheath flow in the rest of the column. The walls are wetted with demiwater and can be warmed to high temperatures. The relative himidity at the walls is 100%. The principle of the supersaturation column is based on the fact that diffusion of heat in air is slower than the transport of water vapor itself (DMT, 2012). Water vapor from point B transports to the dried aerosol sample in point C, while the heat from point A diffuses to the same aerosol sample in point C. Since this heat diffusion is slower, the temperature in the middle of the column is lower than the dew point and the relative himidity excees 100%. This supersaturation makes the water vapor condense on the aerosol sample, creating cloud particles. The temperature gradient on the column can be adjusted in such a way, that the amount of supersaturation can be chosen. Using these degree of freedom, the aerosol sample is exposed to 5 levels of supersaturation, creating a specific amount of cloud particles for every level of supersaturation. These cloud particles are consecutively transported to a particle counter similar to the CPC in the SMPS.

This device gives information about the potential cloud formation for the sampled aerosol, in various supersaturation scenarios. Therefore, this device represents great importance for the Ruisdael project. The sample flow is set to be 0.5 liters per minute.

4.4.9 ACSM

The Aerosol Chemical Speciation Monitor (ACSM) is used to measure the chemical composition of the aerosol particles in the air. In contrast to the SMPS, the ACSM works independently of particle sizes. The aerosol sample is focussed into a particle beam inside an aerodynamic lens. The particles are beamed onto a hot sheet, placed in a vacuum environment. The hot sheet in vacuum will cause the particles to evaporate. The particle vapour will consenquently experience an electron beam, resulting in ionization and fragmentation. By introducing a electrical potential, the ionized fragments and molecules will be transported through a mass spectrometer. By analyzing the masses of the molecules and fragments, information about the chemical composition of the particles is gained. More specific information of the ACSM is not discussed, for the device has not arrived by the time this thesis was written.

4.4.10 Laboratorium

The measurement devices have to be stationed inside, therefore a new laboratorium is placed next to the Lutjewad tower. The outer inlet as displayed in figure 8 is completely stationed outside, while the inner inlet from figure 10 is almost completely stationed on the inside. A sea container is designed and used as laboratorium. A schematic drawing of the container placement is seen in figure 15.

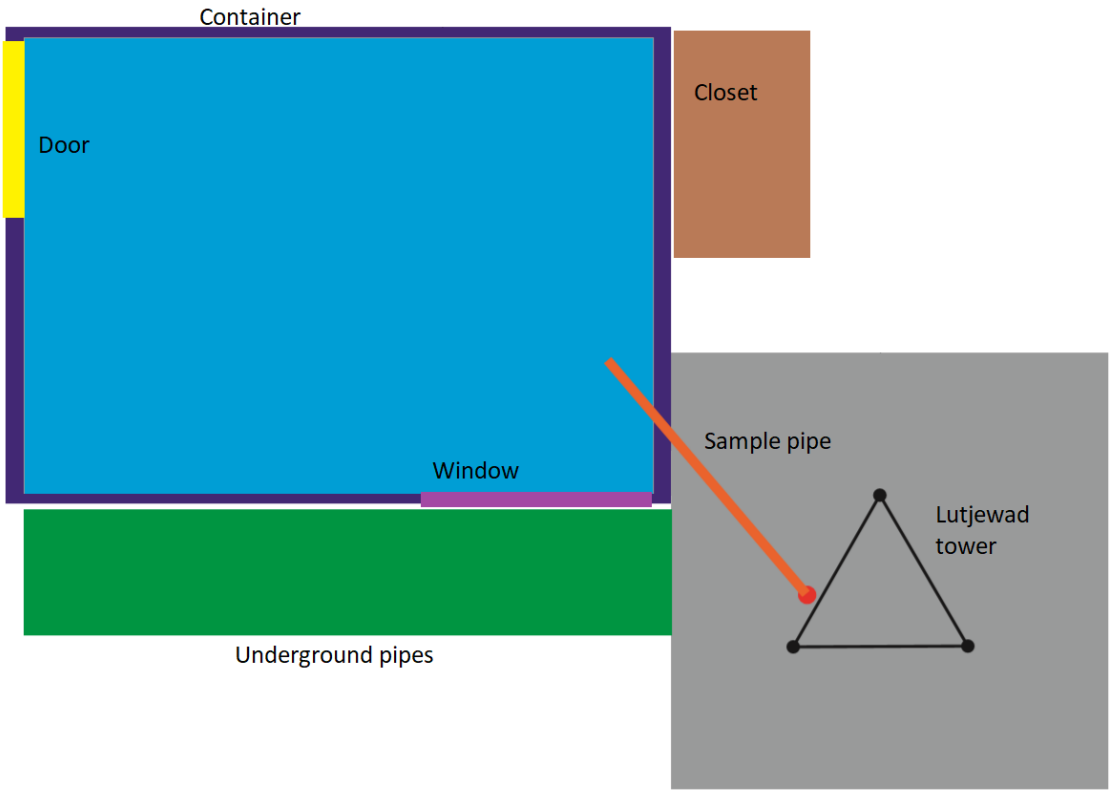

Figure 15: Schematic top view of the placement of the container with respect to the Lutjewad tower. This picture is on a relative scale.

The outer dimensions of the container are 2991 x 2438 x 2591 mm (length x width x height). This container is insulated and equipped with heating and airconditioning. In this way, the climate in the container can be kept stable, in order to maximize the the performance of the measurement devices. For the same reasons, the colour of the container is chosen to be white (colour code: RAL9010). This is done to prevent the container from heating up too much during summer time.

For practical reasons, a small door (yellow) and window (purple) are placed in the container to create a pleasant workspace. The placement of the container was restricted to be outside the green area, for underground pipes and tubes are placed to connect the Lutjewad tower with the main laboratorium. The red dot next to the Lutjewad tower represents the mainpipe, which is vertically attached to the tower. The orange part indicates the sample pipe. Other parts are for clarity not shown in this figure.

As seen in figure 15, the sample pipe intersects the rear wall of the container with an angle. Hence, an opening in the container is created at a similar altitude as the bottom end of the main pipe. This gap area is 500 x 260 mm (height x width), in order to have enough working space to insert the sample pipe into the main pipe and be able to remove it.

Underneath this sample pipe gap area, another gap area is constructed. This gap area is used for all the cables and tubes that enter or leave the container. Cables for electrical power and data, as well as tubes for compressed air.

The sample pipe enters the container between connections C9 and C10 (figure 10). Hence, the nafion dryer is the first part of the inlet that is completely inside the container. The manifold and the measurement devices are also inside the container, as well as the small flow controller and pump (flow controller 2 and pump 2). The compressor and adsorption dryer that provide the dry counter flow, however, are placed in the Lutjewad main building, transporting the dry air through an underground tube to the container. This is done to avoid noise disturbance inside the container. Besides, the compressor and adsorption dryer from this project will be used as the main compressor for the Lutjwad station: more devices will be connected to this drying segment. The larger flow controller and pump (flow controller 1 and pump 1 from figure 8) are placed outside the container, in a closet (brown area in figure 15) right next to the container. This is also done to prevent noise disturbance, since the large pump produces significantly more noise. The placement of the SMPS, CCN counter and ACSM inside the container is to be decided. No optimal placement was found yet during the time this thesis was written.

To prevent the container from sinking into the ground, a suitable foundation is placed underneath the container. This foundation is capable of bearing over 6000 kilograms, even though the container itself is merely 1500 kilograms. The container is also grounded, to prevent the destroying of the infrastructure by a lighting bolt. More pictures of the laboratorium can be seen in the Appendix.

5 Aerosol transport efficiency Model

In this chapter, the equations from section 3 are applied to the specific inlet explained in chapter 4 to estimate the particle transport efficiency as a function of particle diameter. The aerodynamic particle diameter is used (section 3.1). The range of particle diameter is chosen to be between 10 nm and 2.5 μm ($1 \cdot 10^{-8}$ to $2.5 \cdot 10^{-6}$ m) and is plotted on a logarithmic scale. This lower boundary is chosen since the measurement devices cannot measure particles lower than 10 nm. Besides, the empicical parameters in the equation for the slip correction factor Cc (equation 7) does not fit the smallest particles very well (Kim et al., 2005). The upper boundary is chosen based on the aerosol entrance. This is a PM2.5 entrance, which means that particles up to 2.5 μm can flow though the entrance, while larger particles will be removed. Details about the entrance can be seen in chapter 4

The physical dimensions of all the parts are given in the Appendix (table 2). For this model, the air is assumed to be in standard conditions: The air temperature is room temperature ($25°C = 293\ K$) and the pressure is 1 $atm = 1.01\ bar$. This defines the density and viscosity of the air as well. All the parameters used in the model can be seen in the Appendix (table 1)

The model exists of four efficiency calculations in four different parts of the inlet. The 4 parts that are used in the model are all the parts where the sample flows through towards the SMPS. The parts are the following: the main pipe, the sample pipe, the manifold and the last tube towards the SMPS.

5.1 Diffusion modelling

The efficiency of the aerosol transport due to diffusion is calculated with equation 8. As said in section 3.4, it is expected that smaller particles have a lower efficiency. Diffusion happens in all the modelled parts, making it an important factor. In figure 16 the modelled efficiency is seen.

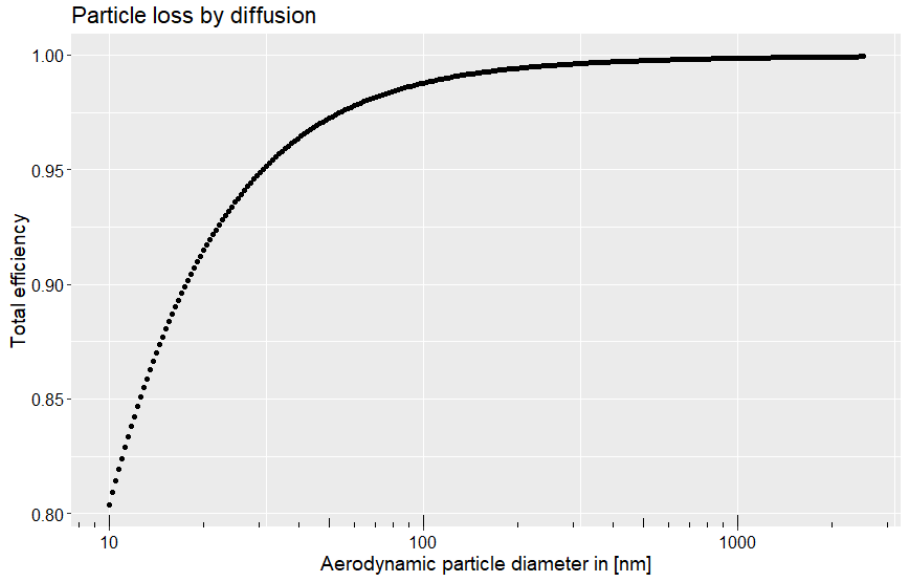

Figure 16: Result of the modelled transport efficiency by diffusion.

As expected, diffusion has a more significant effect on smaller particles compared to larger ones. For the smallest ones, around 20% of the particles will be lost. The larger the particle is, the higher the efficiency. Diffusion cannot be prevented, although it could be minimized. An higher efficiency could be achieved by decreasing the residence time in the pipes, i.e., increasing the sample velocity. In that case, more of the sample already reaches the measurement devices before part of the sample is lost.

5.2 Gravitational settling modelling

Gravitational settling only occurs in parts of the inlet where the aerosol is transported horizontally. As seen in section 4.3, the main pipe and the first part of the sample pipe are placed vertically. In these parts, there will be no gravitational settling, so the efficiency is 100%. Equation 12 is used to calculate the efficiency, which is seen in figure 17.

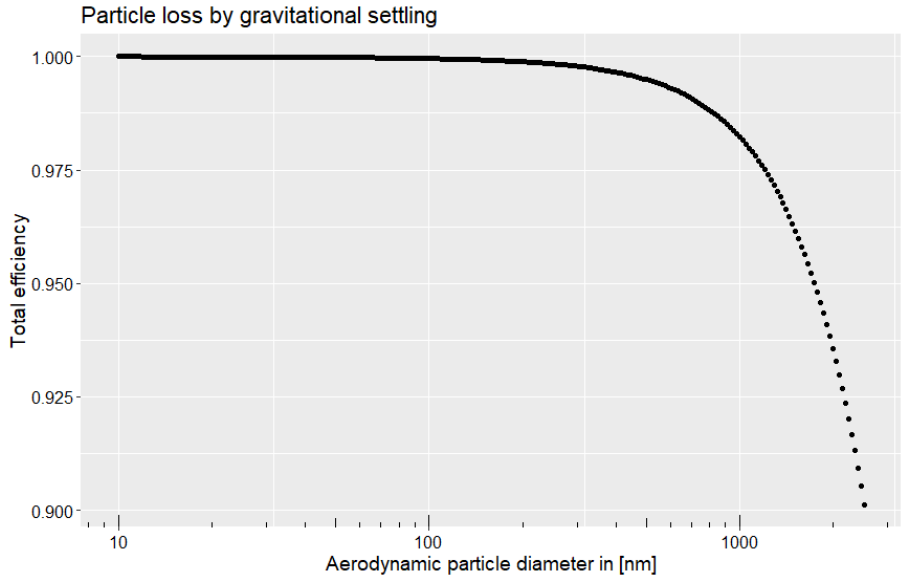

Figure 17: Result of the modelled transport efficiency by gravitational settling.

As expected, gravitational settling mostly occurs for larger particles. For the upper limit, at 2.5 μm, almost 10% of the particles are lost. Gravitational settling is therefore one of the most important causes of particle loss, although this only occus in the horizontal part of the inlet. Between 10 nm and 100 nm, there is no particle loss by settling. The efficiency can be increased by decreasing the residence time in the inlet, just like the efficiency by diffusion. More of the sample would be reaching the devices before gravity affects the particles.

5.3 Impaction modelling

In the inlet, one turn of 90° is made comparable to figure 4. The sample pipe begins vertically, but after the turn it continues horizontally. In this model, this is the only place for potential particle loss by impaction. Equation 14 is used to model the efficiency as seen in figure 18.

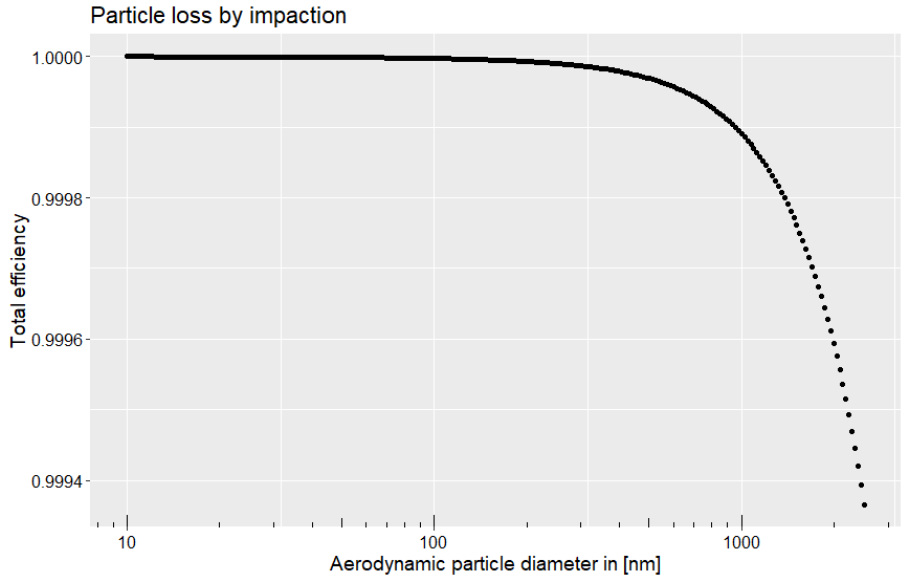

Figure 18: Result of the modelled transport efficiency by impaction.

Just like gravitational settling, impaction affects larger particles the most. The scale however is entirely different. The relevance of impaction in this inlet is completely negligible compared to diffusion and gravitational settling. If the sample velocity would be drastically increased or a PM10 entrance would be installed, this could become a more significant factor. In this case, an higher velocity would decrease the efficiency, in contrast to diffusion and gravitational settling.

5.4 Isokinetic subsample modelling

Lastly there is the isokinetic subsampling. From the main pipe into the sample pipe. As shown in section 4.4.5, there is a superisokinetic subsampling situation (subsample velocity is higher than initial sample velocity, figure 6). The relative difference between the velocities are however well between the boundary conditions from section 3.7. Superisokinetic subsampling means that the larger particles cannot follow the streamlines like the smaller particles, resulting in a particle loss for larger particles. Equation 15 is used to calculate the associated losses and the resulting transport efficiency are shown in figure 19.

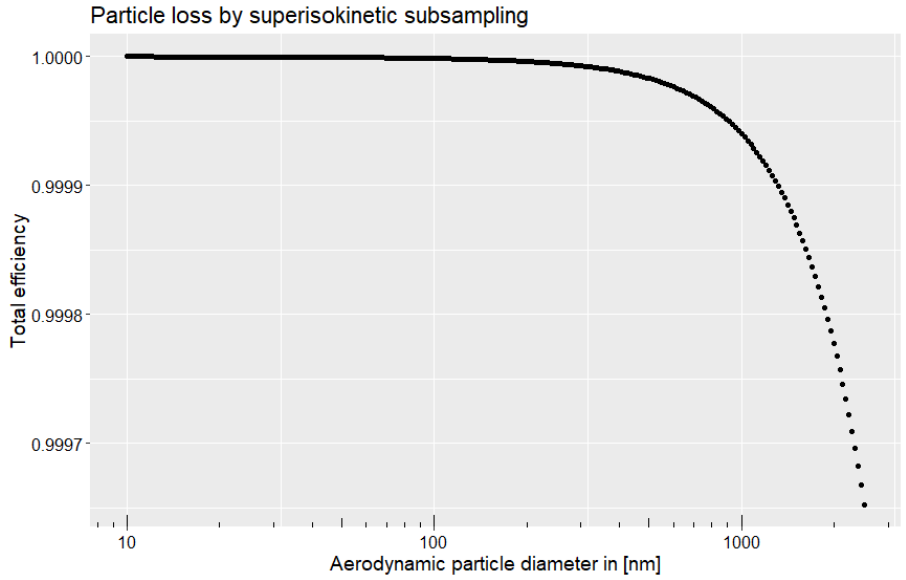

Figure 19: Result of the modelled transport efficiency by superisokinetic subsampling.

As expected, some losses appear at larger particles sizes. The scale however shows that the losses of the superisokinetic subsampling is completely negligible. This shows that even if the velocities of the sample flows differ to a larger degree, losses will presumably not become significant. Similar to impaction, superisokinetic subsampling could be a significant factor if the entrance would be replaced for a PM10 entrance, or if of the sample flow velocitiy would be drastically increased.

5.5 Total aerosol transport efficiency modelling

Combining the particle losses due to all the mechanisms in all the 4 modelled parts of the inlet, the total transport efficiency is calculated. Since the significance of diffusion and gravitational settling is orders of magnitude higher compared to impaction and isokinetic subsampling, the total efficiency will mainly be the result of the first two. The total modelled efficiency is displayed in figure 20, using equation 17.

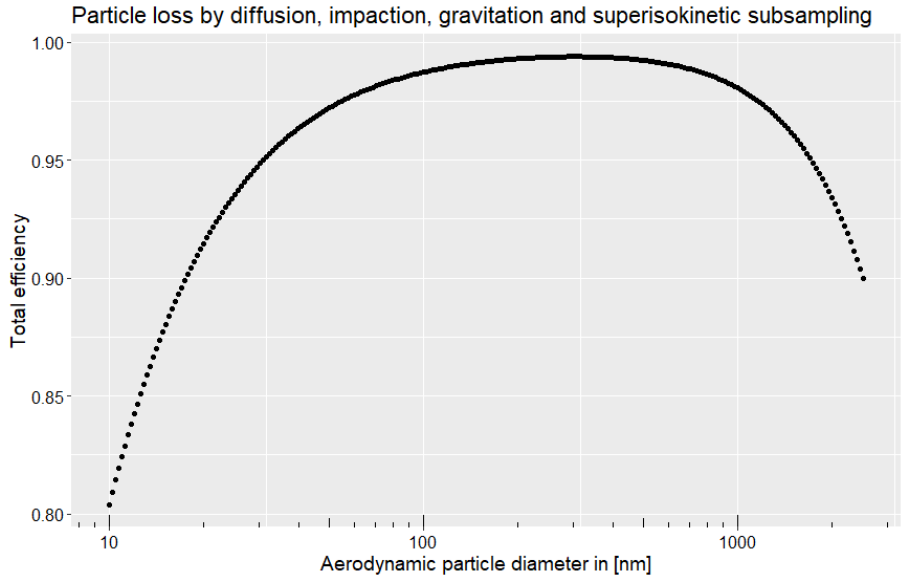

Figure 20: Result of the modelled particle loss by diffusion, impaction, gravitational settling and superisokinetic subsampling.

The total efficiency as seen in figure 20 displays mainly the combined effects of diffusion and gravitational settling. Over the whole range of particle size, there are losses. The smaller particles are affected by diffusion, while the larger ones are affected by gravitational settling. As explained above, the efficiency could be higher for those two phenomena if the sample velocity would be increased. However, the efficiency due to impaction and superisokinetic subsampling would be decreased. Secondly, the flow could become turbulent by an higher flow velocity (section 3.2) since the the Reynolds number Re depends on flow velocity (equation 1). Besides, a low efficiency is not a drastic problem, as long as it is known to the user of the data. Since the data must be corrected for the known particle losses, the quantification of the efficiency is crucial.

6 Calibration

In order to test the particle loss model from chapter 5, a calibration is performed to find the actual particle losses in the inlet. Ideally, the whole inlet as described in chapter 4 is calibrated. Practically, however, there was much difficulty in finding a way to calibrate the whole inlet. Since a calibration of the whole setup was not realistic, only the inner part of the inlet is calibrated.

6.1 Calibration setup

The part of the inlet that is calibrated, is seen in figure 21 as a schematic representation.

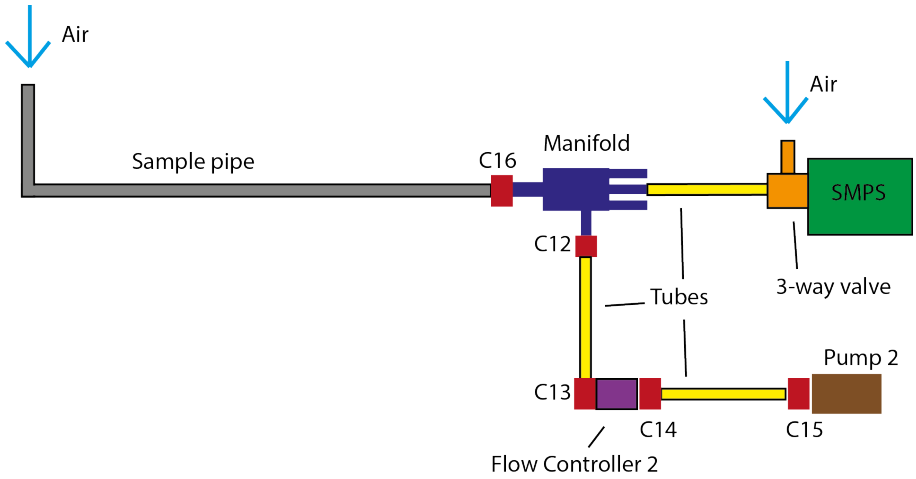

Figure 21: Schematic representation of the calibration setup. The calibration setup starts with the sample pipe, continuing to the manifold. A 3-way valve is placed between the SMPS and the manifold, creating two different routes to the SMPS. The flow controller and pump provide the right amount of flow through the system.

As can be seen in figure 21, the setup starts with the sample pipe, which is continued to the manifold, a 3-way valve and finally the SMPS. The bypass of the manifold is connected to a flow controller and a pump, assuring the flow through the system. The setup is rather similar to the inner inlet from section 4.3.2, although the calibration setup lacks the drying segment. A different connector C16 is used to connect the sample pipe to the manifold. In comparison with the inner setup, the 3-way valve is supplementary. This 3-way valve is crucial for the calibration setup since it provides the option to either connect the setup to the SMPS or to connect the outside air to the SMPS directly. After a sample is taken via the setup, the valve is switched and the outside air is analyzed by the SMPS. The size distributions can now be compared to see whether there is particle loss in the setup. Before this can be done, potential losses in the 3-way valve itself should be investigated as well, since this part is not included in the final setup. This is done in a similar way: By removing and attaching the valve after several size distribution measurements, the size distributions can be compared again. The 3-way valve is a ball valve, meaning that the

valve is capable of transporting aerosol. A picture of the connection of the ball valve is seen in figure 22.

Figure 22: Zoom on the connection from the manifold to the SMPS via the 3-way valve. The valve is now pointed to the setup.

In figure 23 an actual picture the calibration setup is seen. More pictures are found in the Appendix, chapter 11.

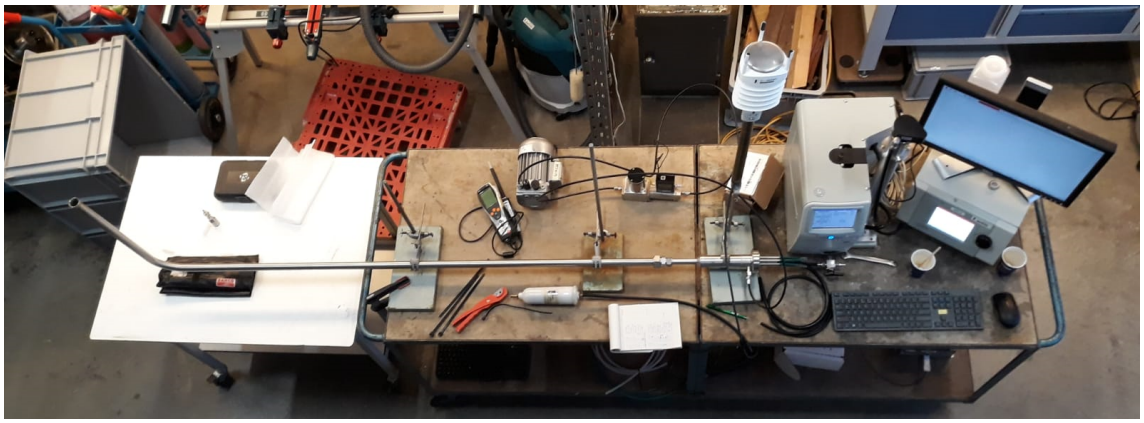

Figure 23: Picture of top view of the calibration setup. From left to right the sample pipe is seen, which is attached to the manifold. All the manifold exits are closed but one, which is attached to the 3-way valve.

6.2 Calibration hypothesis

Regarding the calibration setup as explained in section 6.1, a specific hypothesis is made. Firstly, the hypothesis of the valve transport efficiency is explained below.

Although the 3-way valve is a ball valve, the sample air has to make an turn of 90 degrees in order to reach the SMPS inlet. From sections 3.6 and 5.3, it is known that especially the larger particles can be impacted. Since the SMPS has a detection range between roughly 20 nm and 550 nm, impaction is assumed to be negligible. This range also implies a negligible measureable particle loss by gravitational settling, as explained

in sections 3.5 and 5.2. The valve itself is only a few centimeters long, so the residence time inside the valve is rather small. From sections 3.4 and 5.1 it is learned that losses by diffusion are low for a short residence time. Combining all those assumptions, the hypothesis is that no significant particle losses are present inside the valve itself. This means an efficiency of around 1 (100%) for all particle diameters.

Focussing on the setup, it is - for the same reasons as above - assumed that gravitational settling and impaction for this particle size range is negligible. The residence time in the setup is much longer compared to the residence time in the valve however, thus diffusion is likely to induce particle loss. Using the same model as in chapter 5, a specific effiency due to diffusion is calculated for this specific calibration setup. This is shown in figure 24.

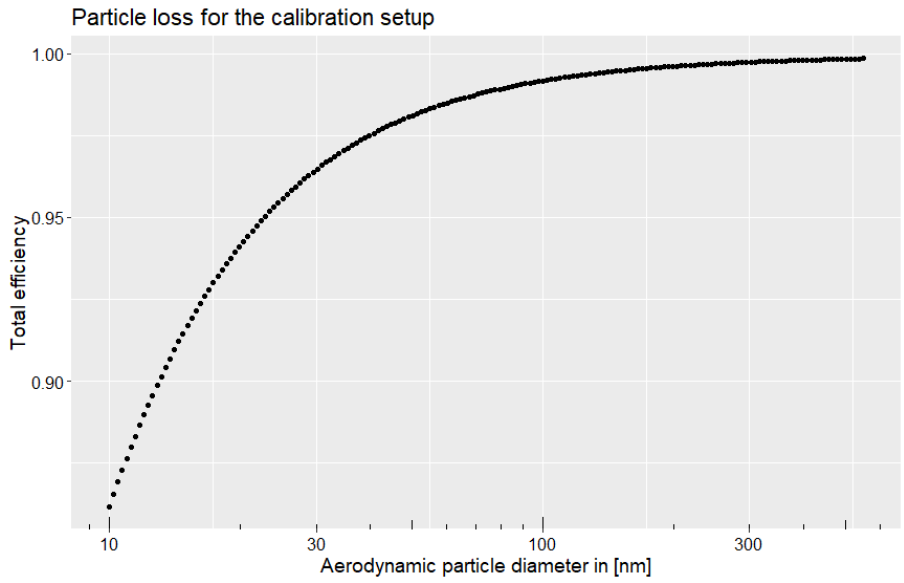

Figure 24: Hypothesis of efficiency in the calibration setup. Only particle loss due to diffusion is seen. The particle diameter range is adjusted to the range of the SMPS.

Figure 24 resembles with figure 16, with the exception that the diffusion in the main pipe is not modelled. The efficiency for the smaller particles is around 87%, instead of the 80% in the whole setup. Measurements are repeated to reach the lowest uncertainty possible (as explained in section 3.9). It is expected that the measured values will follow the same trend as figure 24, although in reality the particle losses are expected to be more significant, i.e., the model describes a perfect system, while the real calibration setup - by definition - has flaws.

6.3 Calibration method

For both the valve and setup calibration, the SMPS is used making scans of the ambient particle size distributions. Every scan measures the amount of particles for 97 different particle diameters, in a range from 17.5 nm to 552.3 nm. One scan of the particle size distribution takes 90 seconds. Five scans are made for each setting of the valve, i.e., five

scans where the air is drawn through the setup, five scans where the ambient air is drawn directly into the SMPS. Five scans later, the route is changed back to the initial state. A set of five scans is called a "run". This means that about every eight minutes, a new run is started. A mean and uncertainty of the particle size distributions is calculated for every run. To find the efficiency of the valve, the ratio is calculated between the amount of particles where the air is drawn through the valve (Route A) and without using the valve (Route B). To find the efficiency of the setup, the ratio is calculated between the amount of particles where the air is drawn through the setup (Route A) and without using the setup (Route B). This can simply be calculated using equation 22.

$$\eta_{cal} = \frac{n_{Route\ A}}{n_{Route\ B}} \tag{22}$$

Where $n_{Route\ A}$ is the amount of particles in $\frac{dN}{dlogDp}$ where the air is drawn either from the 3-way valve or the setup and $n_{Route\ B}$ is the amount of particles in $\frac{dN}{dlogDp}$ where the air is drawn either without the valve or without the setup. Finally, η_{cal} stands for the total efficiency of the calibration. Since aerosol of open air is variable, the calibration is performed indoors in a large room without direct influx of external air. Nevertheless, there will be a change in particle size distribution over the measurement time. Equation 22 is therefore only used for runs that are consecutive, e.g., the relative difference between run 1 and 2, run 2 and 3, et cetera. This implies that for n runs, $n-1$ efficiencies can be calculated. Since the runs follow each other within ten minutes, particle size distribution of the aerosol is assumed to not have changed so much. Besides that, by comparing every consecutive run, a trend can be accounted for. This is displayed and explained more clearly in section 6.4.2 (figure 29).

6.4 Calibration results and discussion

6.4.1 Valve transport efficiency

For the valve transport efficiency, ten runs (i.e. 50 scans) are completed. Using equation 22, the efficiency is calculated nine times for every particle diameter. The mean efficiencies and errors are calculated as described in section 3.9, resulting in figure 25.

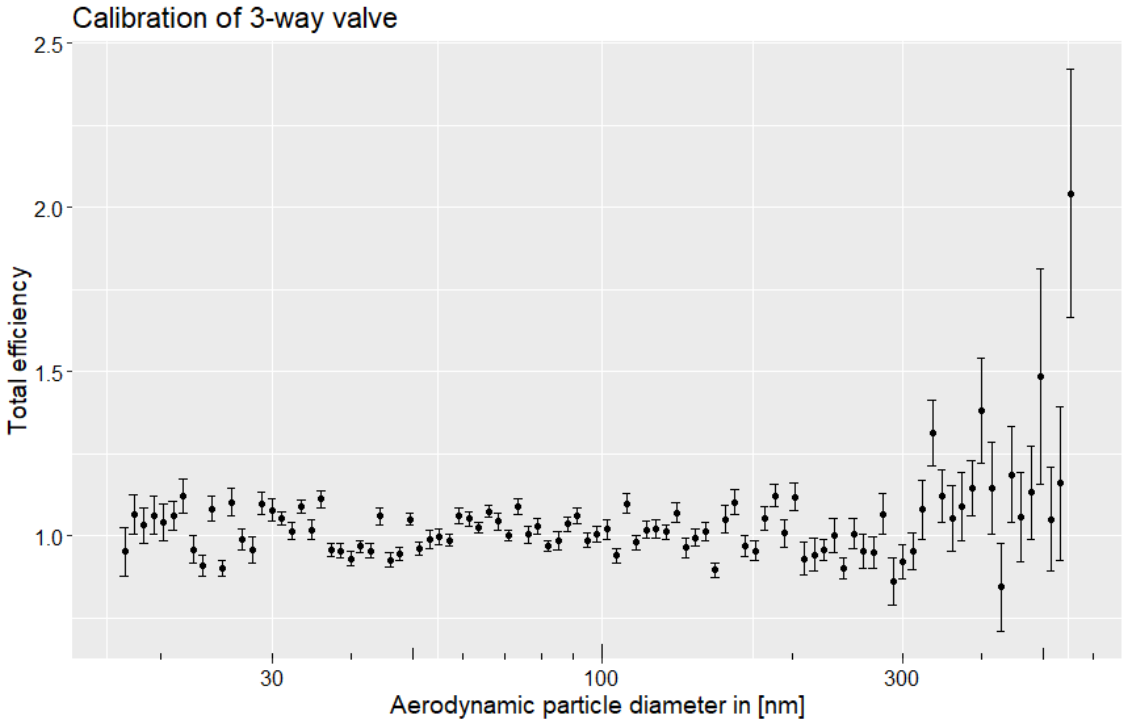

Figure 25: Efficiency of the 3-way valve as a function of particle diameter Dp.

According to the hypothesis from section 6.2, the efficiency should be 1 (100%) for every particle diameter. For the smaller particles ($17.5\ nm < Dp < 300\ nm$), the datapoints are - as expected - well around 1. The larger particles ($300\ nm < Dp < 550\ nm$) display a drastic increase in uncertainty. Essentially, the SMPS counts particles with a certain electrical mobility diameter (section 4.4.7). This implies that the statistical analysis for particle sizes with a natural low concentration, such as larger particles, is less accurate. Therefore, the efficiency will from now on only be displayed for $17\ nm < Dp < 300\ nm$.

The error bars in figure 25 represent the standard errors from equation 19. The uncertanties however are not entirely independent, as the particle size distribution in the ambient air can drift towards a changed particle size distribution. This implies that the displayed errorbars underestimate the true uncertainty.

6.4.2 Experimental calibration setup

To calibrate the setup, 30 runs (i.e. 150 scans) are completed. This results in 29 efficiency calculations using equation 22 for every particle diameter between 17.5 and 300 nm. To make a proper comparison between the theoretical modelled efficiency from figure 24 and the measured efficiency, both of them are plotted in figure 26.

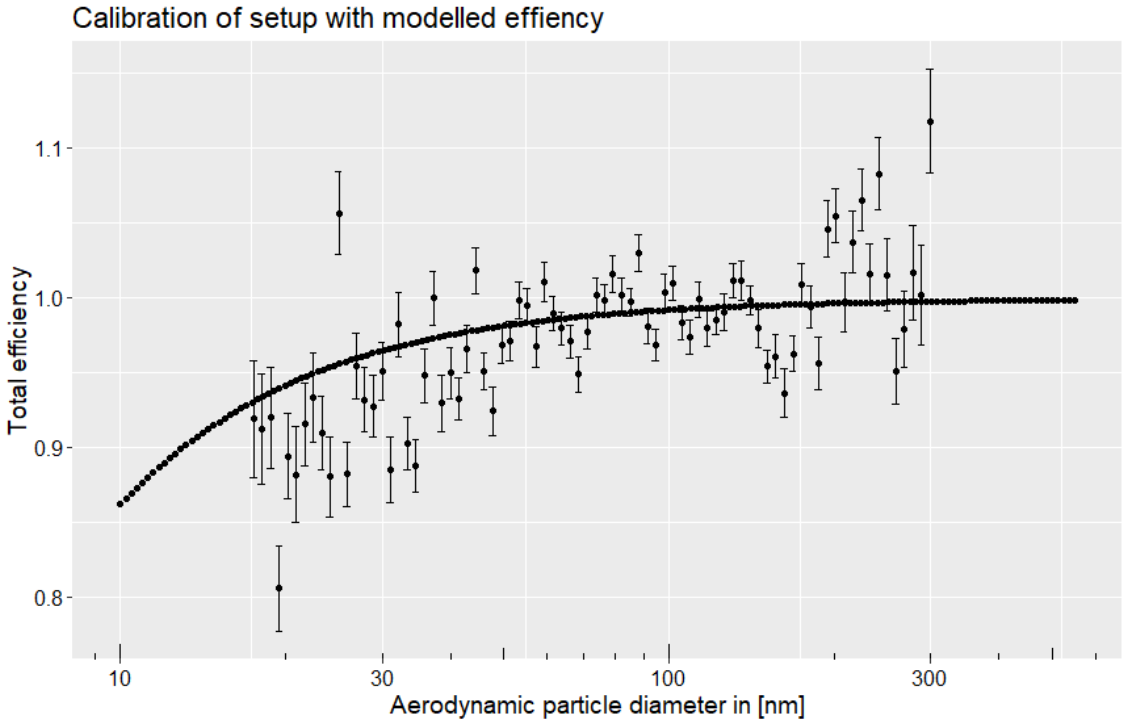

Figure 26: Efficiency of the setup and the modelled efficiency as a function of particle diameter Dp.

From figure 26, a trend is seen in the measurements that smaller particles have a lower efficiency. This trend is comparable to the modelled efficiency trend, displayed in the same figure. For the middle to greater particles ($55\ nm < Dp < 300\ nm$) the measurements fit the model fairly well, while the measurements of the smallest particles ($17.5\ nm < Dp < 55\ nm$) are significanlty lower than the modelled values. The lower efficiency in reality is in line with the hypothesis from section 6.2, since the model assumes a perfect setup, while the real setup has flaws.

The error bars are calculated in a similar way as explained in section 6.4.1, which means that the errorbars again underestimate the true uncertainty. To display the drift of the particle size distribution and the dependency of the measurements, figure 27 is composed.

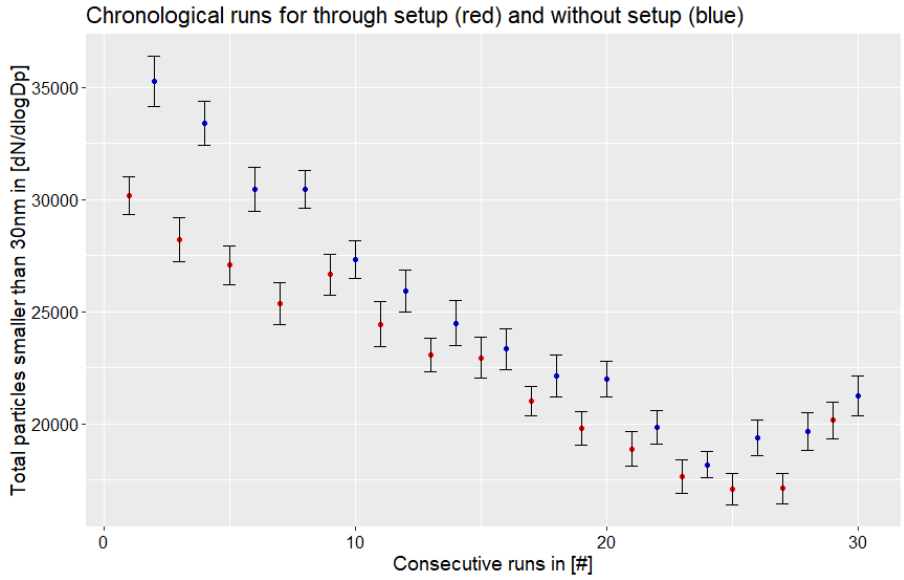

Figure 27: Total amount of particles smaller than 30 nm for every consecutive run. The red series represent the runs through the setup and the blue series represent the runs without the setup.

Figure 27 shows the total particle concentration (in dN/dlogDp), averaged per run. The runs are orderded chronologically. The error bars are standard errors (equation 19). The particle loss in the setup is clearly seen, as the red series in general has a lower particle concentration. A general decreasing trend is seen as well, meaning the total particle concentration ($17.5\ nm\ <\ Dp\ <\ 30\ nm$) decreases over time. This proves the dependencies of the datapoints. A similar plot focussing on larger particles is seen in figure 28.

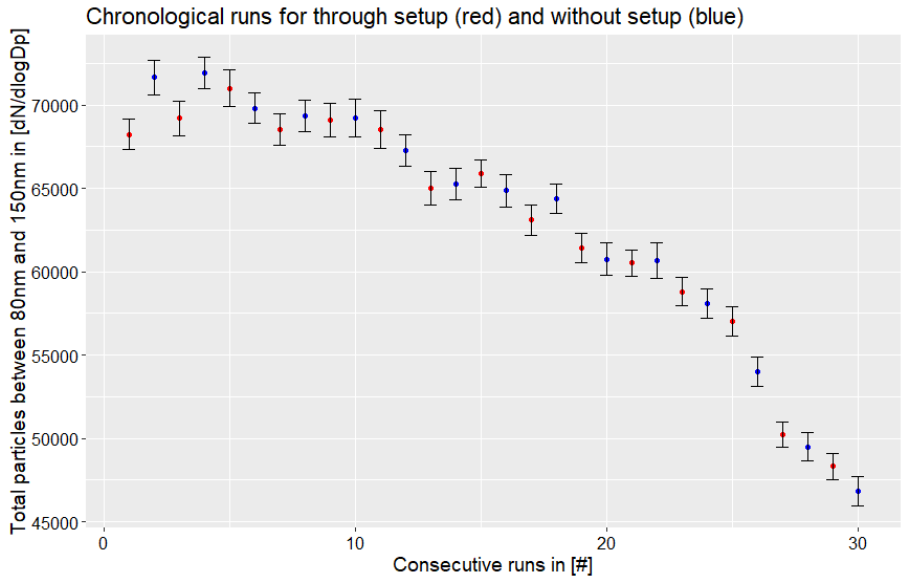

Figure 28: Total particles between 80 and 150 nm for every consecutive run. The red series represent the runs through the setup and the blue series represent the runs without the setup.

Similar to figure 27, figure 28 displays a general decrease of particle concentration. For these particle sizes however, there is no particle loss seen between setup and no setup. In this way the particle loss for small particles is confirmed, despite the changing aerosol population (i.e. particle size distribution in the ambient air).

By calculating the efficiency between every run, the decreasing trend is accounted for. This is displayed quite schematically in figure 29.

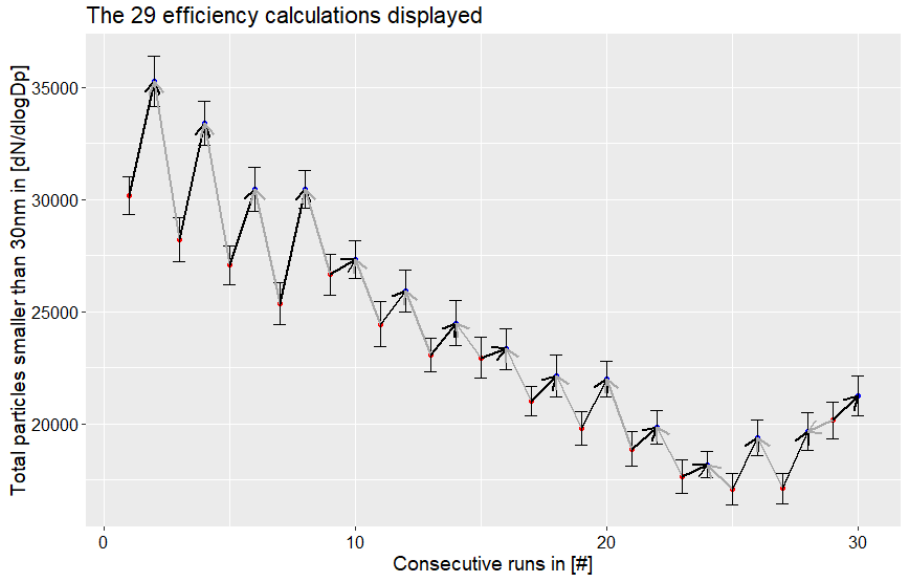

Figure 29: Display of every efficiency calculation. Every arrow represents an efficiency calculation between the two runs.

Since the total efficiency is calculated as the mean of all the efficiencies, figure 29 could be seen as a representation of the efficiency for particles with sizes between $17.5\ nm < Dp < 30\ nm$. The mean of all those arrows has a nonzero vertical component, implying a net particle loss. If only the black arrows are used to calculate the efficiency, the drift would have a large effect on the data. Therefore, the black and the grey arrows are used to find the efficiency, correcting for the drift in the particle size distribution. Although statistical measures can help correcting for a drift in the population, the true uncertainty will still be underestimated by the calculated standard error. It could be possible to perform more corrections on the data, e.g., the exclusion of outlying measurements or scans, although the result will not necessarily be better. After all, the initial calibration of the setup does fit the modelled values (figure 26) in the way expected in the hypothesis (section 6.2). The calibration will be further discussed in section 7.3.

7 Discussion

In this chapter, the inlet from chapter 4, the model from chapter 5 and the calibration from chapter 6 will be discussed.

7.1 Discussion on the inlet

In retrospect, the inlet built in Lutjewad has some flaws. The main pipe, although welded using the orbital welding technique, still has small ridges. In particular the larger particles can be deposited on these edges. Besides, the flow can become locally turbulent, resulting in more particle loss. The outer and inner diameter dimensions of the main pipe are non standard. This meant that the order of the pipes were more expensive, as well as the connections to the main pipe. Especially connector C1 was significantly more expensive compared to other connectors. On top of the expenses, the diameter of the main pipe was arbitrary, i.e., the pipe could have been slightly larger or smaller. As long as the flow would be easily within the laminar regime, the dimensions itself can be chosen. This makes the high expenses of connector C1 even more futile.

The top part of the sample pipe is not wide enough to create an isokinetic subsampling system. Although the particle losses are calculated to be extremely low, the diameter of the top part was ideally 1 mm wider.

The nafion column that was constructed by the company Tropos has an in- and oulet diameter of $\frac{3}{8}$ inch. The placement of this nafion column is between the sample pipe (1 inch diameter) and the manifold ($\frac{3}{4}$ inch diameter). These inconvenient dimensions make it inevitable to have connectors C10 and C11 (from figure 10). These connectors are respectively convergent and divergent, inducing extra curvatures. It is advised to replace the in- and outlet of the nafion dryer to respectively 1 inch and $\frac{3}{4}$ inch. Supplementary (smaller) nafion dryers are ordered to dry the sample between the manifold and the measurement devices if necessary.

7.2 Discussion on the model

The model from chapter 5 is specifically designed for the inlet described in chapter 4. If the inlet is adjusted or adapted, the model will have discrepancies. All the dimensions of the inlet and assumptions used in the model are listed in the Appendix.

The nafion dryer (section 4.4.3) is not included in the model. Although the nafion column is expected to have very low particle losses (Wiedensohler and Birmili, 2019), the addition of the modelled particle loss in the nafion column would further complete the model towards reality.

The assumptions concerning the standard conditions such as temperature and pressure of the sampled air are debatable. The inlet samples air during all seasons, thus the conditions of the sampled air differ extremely. For example, at ground levels the temperature in the nearby village Lauwersoog was measured between -1.1 °C in January and 20.1 °C in

August 2019 (Climatedata.org, 2019). When temperature and pressure of air are mutated, the viscosity (η_{air}) and the density (ρ) of the air are influenced as well. For example, the diffusion coefficient in equation 4 and the relaxation time in equation 11 are dependent on the viscosity of air η_{air}. A better model would include several temperature and pressure levels, to account for the volatility of the conditions.

The particle transport efficiencies as modelled in this thesis are calculated assuming perfect pipes and tubes. In reality, the inlet is not perfect. Impurities like edges or rough surfaces induce more particle loss in practise, which is not accounted for in the model. For example, additional particle losses can occur due to the flow type: The model assumes a laminar flow, so the efficiency equations for laminar flow are used. A turbulent flow induces the use of different equations, altering the outcome of the model as well. The modelled value can therefore be considered as the theoretical maximum efficiency.

As mentioned in chapter 5, the numerical value for the slip correction facter C_c is questionable for particle with a small diameters (Kim et al., 2005). Diffusion is more significant for smaller particle diameters, resulting in an uncertainty in the outcome of the calculations. The uncertainty is the largest around a particle diameter of 1 nm, since the particle is about the size of a single molecule. This makes the assumption of spherical particles rather implausible, so the extrapolated empirical values of the parameters from equation 7 are less convincing. Although the slip correction factor is more satisfying for 10 nm particle diameters, some caution in this part of the model is advised.

To further perfect the model, better software can be used. Flow dynamics can be modelled in a fluid mechanics model program. Such a program was never acquired during this thesis, making it impossible to perform. For future additions or adaptations, however, the use of such software is advised.

7.3 Discussion on the calibration

The calibration as described in this thesis has some flaws. First of all, not all the parts were calibrated: The main pipe and the nafion column were not included in the calibration setup. The main pipe was not included for practical reasons, while the correct connectors for the nafion column were not present yet. This made the addition of connector C16 (setup is seen in figure 21, the connector itself is shown in the Appendix in figure 43) necessary, although it has no place in the final infrastructure. A calibration performed on site with all the parts connected would provide more complete results.

Also, the range of particle diameters is rather small. By focussing on particles of 500 nm and smaller, only the particle loss by diffusion is measured. Particle loss by gravitational settling only occurs significanlty for the larger particles. An experimental setup with a measurement device that can detect the larger particles would be advised to map the efficiency of particle transport due to gravitation, impaction and superisokinetic sampling.

The most notable point of discussion is the changing aerosol concentrations throughout

the experiment. This problem is quite hard to solve. The ambient air changes in time, making the comparison of consecutive samples less trustworthy. For example, the presence of the person executing the calibration changes the aerosol. To solve this, an electrical 3-way valve could be used, that can be managed from a different chamber. However, a valve like this is rather expensive.

To minimize the changing nature of the ambient aerosol, the calibration can be performed in a large, closed environment. In this way, external factors changing the aerosol are excluded. Another effective way to reach a stable aerosol population could be the addition of an aerosol buffer to the system, i.e., a tank filled with air. Samples from this tank are led into the experimental setup, while the buffer tank is in contact with the ambient air. When the ambient air changes due to external factors, the population inside the buffer tank changes minimally. A buffer tank was considered during this thesis, yet it was not used. For the implementation of a buffer tank comes with difficulties. In order to implement the buffer tank correctly, the tank should be attached to the sample pipe and the 3-way valve in exactly the same way. This implies that the buffer should either be physically transported between the sample pipe and the valve, or that two exactly the same tubes should transport the air to the both inlets. The first option is practically difficult, while the second option is deemed unrealistic. It is also not possible to work with two buffer tanks, for a comparison is inaccurate when samples are taken from two different populations.

In the future, a complete and well performed calibration is advised. This calibration should be done at the Lutjewad site itself using the entire infrastructure. The range of particle diameters that are measured should be more wide, i.e., ideally from 10 nm to 2.5 microns, since this is the full range of particles in the system. When a calibration like this is performed, the problem of a closed environment is not solved, however. External influences like a gust of wind or a passing tractor could manipulate the calibration results. Thus, this calibration should be done on a windless day, when no tractors or trucks pass by. Another problem regarding a calibration at Lutjewad is the fact that the aerosol population is not the same at both inlets (the 3-way valve and the aerosol inlet on top of the main pipe). Physical conditions like pressure and temperature differ between the ground level and at a height of 20 meters. Besides, the measurement devices are stationed inside the container, while the aerosol inlet is stationed outside the container. In this way, the samples from both routes are not at all taken from the same population. Further investigation is needed to solve these problems.

8 Conclusion

The objective was to design, construct and test an aerosol measurement infrastructure suitable for the Lutjewad station. The infrastructure needs to satisfy the requirements mentioned in section 4.1. The particle loss in the inlet system should be determined for the entire range of particle diameters in the system and should be as low as possible.

It is difficult to evaluate the design and the construction of the inlet itself, for the actual construction is not entirely completed. Since no major flaws are encountered during the construction so far, the design is deemed to be satisfactory. Many parts are easily replaceable and the inlet itself can be disassembled.

No conclusion can be drawn about the functioning of the entire infrastructure, for the measurement devices are not present yet. Part of the inlet is used during the calibration, however. Since the inlet system designed in this thesis functions properly, the working principle of the design is for the time being deemed satisfactory.

Regarding the particle loss, a model is designed that calculates the reduction in transport efficiency of particles between 10 nm and 2.5 microns due to diffusion, gravitational settling, impaction and non-isokinetic sampling. This model is experimentally tested on one segment of the entire inlet, the sample pipe. Although the experimental setup is only able to measure particle between 17.5 and 550 nm, it is concluded that the model decribes the particle loss in reality sufficiently. The model can be considered as the theoretical maximum efficiency, while the actual efficiency is slightly lower.

To fully map the particle loss in the entire measurement infrastructure, another calibration is advised. This calibration should include all the segments of the infrastructure and particle sizes. After completing the construction of the infrastructure in Lutjewad, the development of a full calibration plan is advised. This calibration could be considered as a thesis itself.

9 Acknowledgements

First of all, I want to thank Ulrike Dusek, PhD for supervising my thesis. The discussions we had about the infrastructure, calibration and data analysis were productive and constructive. I also want to thank Bert Kers for all the practical knowledge and work he put in this project. Together we designed and constructed a large part of the new aerosol infrastructure on Lutjewad already.

My thanks to many others of the Centre for Isotope Research (CIO) institute. Especially dr. ir. Bert Scheeren, Marcel de Vries, Marc Bleeker, Henk Jansen and ing. Jan Mulder. They all contributed to my thesis within their specific field of expertise.

The calibration method and setup was made possible by TNO. Therefore, I want to thank Marcel Moerman and Bas Henzing.

I also want to wish good luck to Xinja Liu and ing. Jan Mulder, who will finalize and use the aerosol measurement infrastructure.

Lastly, I want to thank my family and friends. In particular my wife Irene and my daughter Elin.

10 Bibliography

References

Allen, M. D. and Raabe, O. G. (1985). Slip correction measurements of spherical solid aerosol particles in an improved millikan apparatus. *Aerosol Science and Technology*, 4(3):269–286.

Brèon, F.-M., Collins, W., Fuglestvedt, J., Huang, J., Koch, D., Lamarque, J.-F., Lee, D., Mendoza, B., Nakajima, T., Robock, A., Stephens, G., Takemura, T., and Zhang, H. (2013). *Chapter 8 of Climate Change: Anthropogenic and Natural Radiative Forcing*. IPCC, fifth edition.

Climatedata.org (2019). Klimaat lauwersoog. https://nl.climate-data.org/europa/koninkrijk-der-nederlanden/groningen/lauwersoog-106655/. Accessed: 2019-12-05.

Digitel (2019). Low volume inlets. http://www.digitel-ag.com/de/en/products/low-volume-sampler/low-volume-inlets/. Accessed: 2019-11-12.

DMT (2012). *Cloud Condensation Nuclei (CCN) Counter*. Droplet Measurement Technologies. Manual for Single-Column CCNs.

franshalsmuseum.nl (2019). Jacob van ruisdael. https://www.franshalsmuseum.nl/nl/event/jacob-van-ruisdael/. Accessed: 2019-11-12.

Gormley, P. G. and Kennedy, M. (1948). Diffusion from a stream flowing through a cylindrical tube. *Proceedings of the Royal Irish Academy. Section A: Mathematical and Physical Sciences*, 52:163–169.

Kim, J. H., Mulholland, G. W., Kukuck, S. R., and Pui, D. Y. H. (2005). Slip correction measurements of certified psl nanoparticles using a nanometer differential mobility analyzer (nano-dma) for knudsen number from 0.5 to 83. *Journal of Research of NIST*, 101(1):31–54.

Kulkarni, P., Baron, P. A., and Willeke, K. (2011). *Aerosol Measurements*. Wiley, third edition.

NWO (2019). Ruisdael observatory. http://ruisdael-observatory.nl/. Accessed: 2019-27-9.

Ott, R. L. and Longnecker, M. (2001). *Statistical Methods and Data Analysis*. Brooks Cole, sixth edition.

Sigrist (2019). Isokinetic sample. https://www.photometer.com/en/GlossaryEntry/Isokinetic-sample/. Accessed: 2019-10-10.

S.P. Belyaev, L. L. (1974). Techniques for collection of representative aerosol samples. *Journal of Aerosol Science*, 5(4):325–338.

Tiwary, A. and Colls, J. (2010). *Air Pollution*. Routledge, third edition.

Wiedensohler, A. and Birmili, W. (2019). Actris recommendation for aerosol drying. https://www.wmo-gaw-wcc-aerosol-physics.org/files/actris-recommendation-for-aerosol-drying.pdf. Accessed: 2019-11-12.

11 Appendix

11.1 Tables with parameters and dimensions

Table 1: The parameters that used in the model.

Parameter	**Unit**	**Value**
Air density ρ_{air}	[kg m^{-}3]	1.192
Air temperature T	[K]	298
Air pressure P	[kPa]	102.30
Air viscosity η_{air}	[Pa s]	1.83 $\cdot 10^{-5}$
Particle density ρ_p	[kg m^{-3}]	1000

Table 2: The dimensions of the individuals parts of the inlet that are used to model the particle loss.

	Main pipe	**Sample pipe**	**Manifold**	**To SMPS**
Length in [m]	18	2	0.2	0.5
Horizontal lenght in [m]	0	1.5	0.2	0.5
Inner diameter in [mm]	46	23.4	20	6.35
Volume flow in [l m^{-1}]	38.33	16.7	16.7	0.5
Flow velocity in [m s^{-}1]	0.384	0.647	0.886	0.263

11.2 List of companies

Below the companies are listed that provided parts for the aerosol infrastructure.

Manifold, Nafion dryers, Adsorption dryer, Compressor and the future SMPS:
Leibniz-Institut für Troposphärenforschung e.V.
Permoserstraße 15
04318 Leipzig
Germany

CCN counter:
Droplet Measurement Technologies
2400 Trade Centre Avenue
Longmont CO 80503
USA

Vacuum pumps:
Becker Druk- en vacuümpompen BV
Eurolaan 11
8447 SM Heerenveen
The Netherlands

Flow controllers:
Inacom Instruments
Dwarsweg 71 A
3959 AE Overberg
The Netherlands

Aerosol inlet:
DIGITEL Elektronik GmbH
Illstraße 30
A-6706 Bürs
Austria

Main pipe and welding:
PMF Mechanical
Oosterstationsstraat 16
9981 CE Uithuizen
The Netherlands

Pipe clamps:
K. van der Maar B.V.
Breweelsterweg 6

9978 TE Hornhuizen
The Netherlands

Sample pipe, Connectors C1, C6 to C15:
Swagelok Nederland
Coenecoop 19
2741 PG Waddinxveen
The Netherlands

Bellow, Tee, Connectors C2, C3, C4, C5:
Pfeiffer Vacuum Benelux B.V.
Newtonweg 11
4104 BK Culemborg
The Netherlands

Container:
Dutch Trading Consortium B.V.
Bunschotenweg 127
3089 KB Rotterdam
The Netherlands

Foundation for the container:
Loonbedrijf Harm de Boer
Doctor Schonfeldstraat 2-4
9971 CE Ulrum
The Netherlands

Placement of the container:
Transportbedrijf Heidema B.V.
Rijksweg 87-89
9197 AB Ten Boer
The Netherlands

Outdoor closet:
Rexel
Kieler Bocht 9c
9723 JA Groningen
The Netherlands

11.3 Pictures of the inlet and parts

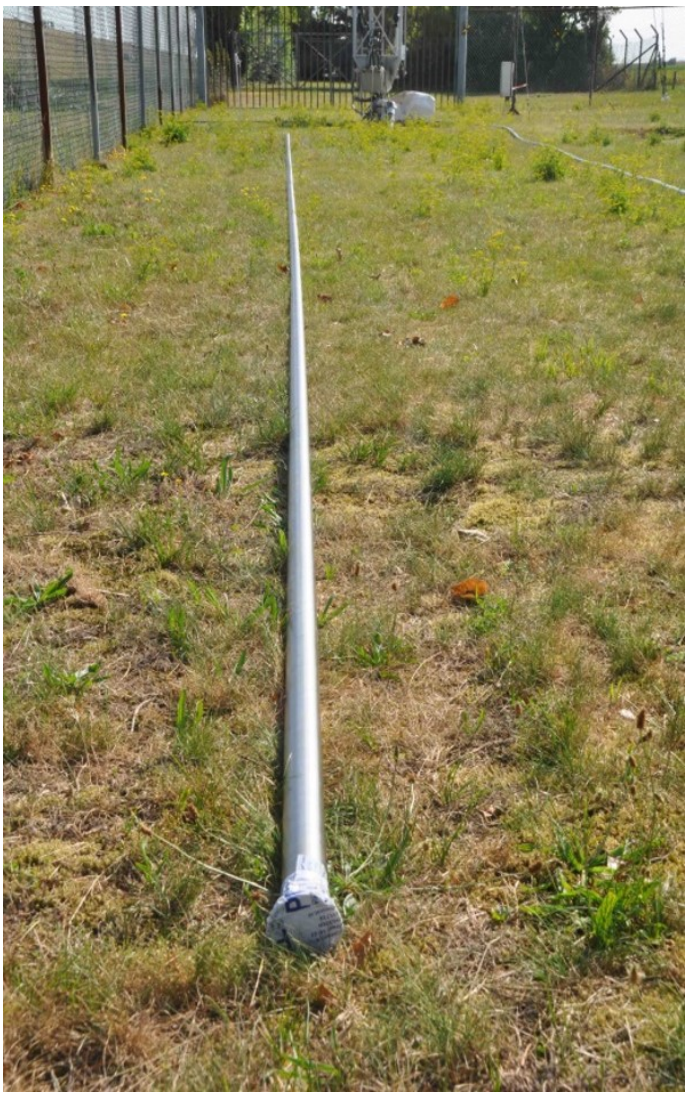

Figure 30: Main pipe lying on the ground at Lutjewad.

Figure 31: Main pipe at the factory.

Figure 32: Close up of orbital weld on the main pipe.

Figure 33: Lower end of the main pipe with the DN50 flange.

Figure 34: The main pipe is attached to the tower using these pipe clamps. The larger part at the left is clamped to the main pipe and the smaller part at the right side is clamped to the Lutjewad tower.

Figure 35: Attaching the main pipe to the Lutjewad tower.

Figure 36: The sample pipe on the floor of the laboratorium in Groningen.

Figure 37: Close up of the manifold. At the left hand side the inlet is seen and at the right hand side the several outlets. The bypass is seen at top top part of the picture.

Figure 38: One of the flowcontrollers used in the setup. The inlet is at the left hand side and the outlet on the right hand side.

Figure 39: One of the pumps used in the setup.

11.4 Pictures of the container

Figure 40: The foundation for the container next to the Lutjewad tower.

Figure 41: The placement of the container.

11.5 Pictures of calibration

Figure 42: Frontal view on the calibration setup.

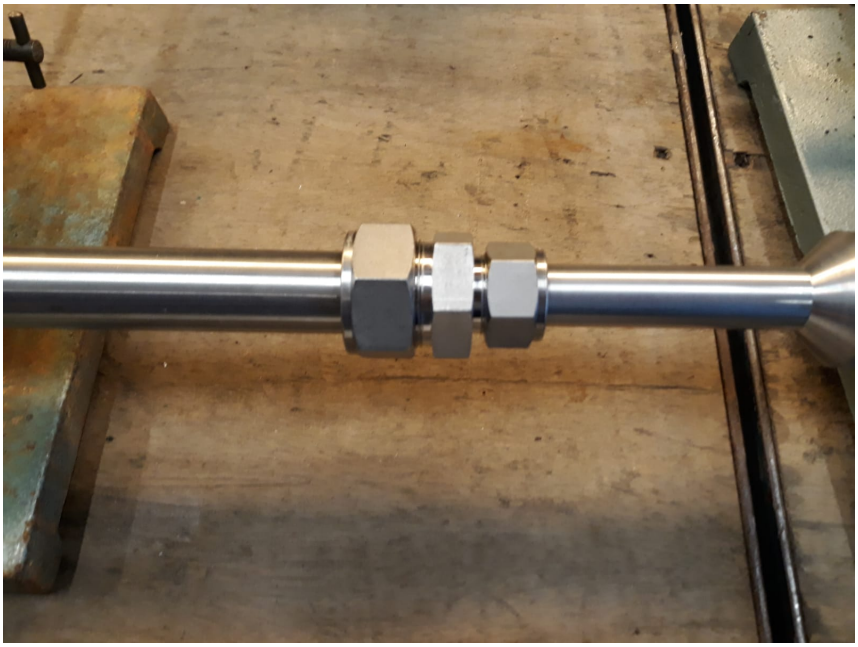

Figure 43: The connection between the sample pipe and the manifold as used in the calibration setup.

Figure 44: The SMPS used for the calibration. Left is the DMA column seen and at the right side the CPC is seen. The SMPS that will be placed in the container at Lutjewad will be different.